



## Full Length Article

# On the origin of reflectance-anisotropy oscillations during GaAs (001) homoepitaxy

J. Ortega-Gallegos<sup>a,\*</sup>, L.E. Guevara-Macías<sup>a</sup>, A.D. Ariza-Flores<sup>a,b</sup>, R. Castro-García<sup>a,b</sup>, L.F. Lastras-Martínez<sup>a</sup>, R.E. Balderas-Navarro<sup>a</sup>, R.E. López-Estopier<sup>a,b</sup>, A. Lastras-Martínez<sup>a</sup>

<sup>a</sup> Instituto de Investigación en Comunicación Óptica, Universidad Autónoma de San Luis Potosí, Alvaro Obregón 64, San Luis Potosí, SLP 78000, Mexico

<sup>b</sup> CONACyT - Instituto de Investigación en Comunicación Óptica, Universidad Autónoma de San Luis Potosí, Alvaro Obregón 64, San Luis Potosí, SLP 78000, Mexico

## ARTICLE INFO

## Article history:

Received 25 October 2017

Revised 22 December 2017

Accepted 28 December 2017

Available online 6 January 2018

## Keywords:

Reflectance anisotropy oscillations

Real-time measurements

GaAs homoepitaxy

## ABSTRACT

We report on the first spectroscopic study of reflectance-anisotropy (RA) oscillations during molecular beam epitaxy (MBE) GaAs homoepitaxy. Real-time RA spectra measured during epitaxial growth were carried out with a recently developed rapid RA multichannel spectrometer with 100 ms per spectrum acquisition time. An analysis of the time-resolved RA spectra shows that RA oscillations are mostly due to the periodic modulation of the surface orthorhombic strain associated to surface reconstruction. Results reported here demonstrate the power of real-time RA spectroscopy as a probe for the study of epitaxial growth processes. In particular, given its sub monolayer surface-strain sensitivity, RA spectroscopy results a very convenient tool to study epitaxial growth mechanisms in real-time with sub monolayer resolution. This capability allows for real-time RA spectroscopy to be used as a probe for the *in situ*, real-time control of epitaxial growth, with the additional advantage of operating in higher pressure systems such as CVD, where RHEED monitoring cannot be implemented.

© 2018 Elsevier B.V. All rights reserved.

## 1. Introduction

The fabrication of advanced optoelectronic devices based on zincblende semiconductors demands for probes with both real-time monitoring and feedback control capabilities for the epitaxial growth process with at least monolayer (ML) resolution. Optical probes would be advantageous for this application given their instrumental simplicity and provided we overcome their intrinsic low surface specificity. Reflectance anisotropy (RA) is an optical polarization contrast technique which enhances the surface-related response by taking advantage of the reduced symmetry of the surface or near surface region of the crystal. RA measures the difference in the optical reflectivity between two principal axis of the crystal, thus suppressing the polarization-independent bulk signal and enhancing the surface response [1].

RA has been applied to study the kinetics of the epitaxial growth of various zincblende semiconductors, demonstrating high sensitivity to the different stages of the growth process [2,3]. In particular, it is known that the intensity of the RA signal oscillates during growth with the same oscillation period as that of specular

RHEED oscillations [4], which is known to correspond to the time necessary to grow one monolayer. RHEED oscillations are widely accepted to be associated to periodic changes in surface micro roughness that take place during layer-by-layer growth [5]. Phenomena leading to RA oscillations, in contrast, are not fully understood. In this regards, on the basis of an effective medium model, Aspnes argues that optical anisotropies associated to surface roughness are too small to explain experimental results and concludes that they have a surface chemistry origin [6]. RA oscillations have also been explained on the basis of a modulation of As dimer coverage during growth as dimers are preferentially broken at island edges [7].


Previous determinations of RA oscillations have been carried out at a single-wavelength or at most a few wavelengths [3,4,7]. However, as it has been shown elsewhere, RA signals may comprise more than one independent component [8,9], hence hampering the physical interpretation of RA oscillations on the basis of single-wavelength data. A deeper understanding of RA oscillations thus demands time-resolved spectroscopic measurements. Carrying out such measurements, nevertheless, demand a rapid RA spectrometer, fast enough to follow in real-time the kinetics of epitaxial growth of III-V compounds (spectrum acquisition times of the order of 0.1 s and  $\Delta R/R$  amplitude in the range  $10^{-3}$ ). Harrison et al., developed a 16 channel rapid RA spectrometer to study the

\* Corresponding author.

E-mail addresses: [jortega@cactus.iico.uaslp.mx](mailto:jortega@cactus.iico.uaslp.mx) (J. Ortega-Gallegos), [alastras@gmail.com](mailto:alastras@gmail.com) (A. Lastras-Martínez).



## Improving titanium dioxide dispersion in water through surface functionalization by a dicarboxylic acid

Victoria González-Rodríguez<sup>a</sup>, Diana Lizeth Zapata-Tello<sup>a</sup>, Javier Vallejo-Montesinos<sup>b</sup>, Ramón Zárraga Núñez<sup>b</sup>, José Amir Gonzalez-Calderon<sup>c</sup> , and Elías Pérez<sup>d</sup>

<sup>a</sup>Maestría en Ciencias Aplicadas, Universidad Autónoma de San Luis Potosí (UASLP), San Luis Potosí, Mexico; <sup>b</sup>División de Ciencias Naturales y Exactas, Campus Guanajuato Departamento de Química, Universidad de Guanajuato, Guanajuato, Guanajuato, México; <sup>c</sup>Departamento de Ingeniería Industrial, Instituto Tecnológico de Celaya, Av. Tecnológico y Antonio García Cubas s/n, Celaya, Guanajuato, México; <sup>d</sup>Instituto de Física Universidad Autónoma de San Luis Potosí (IF-UASLP), San Luis Potosí, México

### ABSTRACT

In this work, we show evidence of improving the dispersion of titanium dioxide particles in water. This is observed in the titanium dioxide-water colloid by the shear-thinning flow behavior in rheological measurements induced by the functionalization of a glutaric acid layer on the surface of titanium dioxide particles. The characterization of the layer was achieved by using infrared spectroscopy and <sup>13</sup>C nuclear magnetic resonance. Rheological measurements corroborated that functionalization of TiO<sub>2</sub> particles decreases the rheological properties such as viscosity measurements at a constant shear rate in two orders of magnitude compared with the pure TiO<sub>2</sub> in suspensions. We present the results as a novel strategy to limit the formation of agglomerates in these colloidal suspensions, and this will be of great use in applications in the paints field and printing technologies.

### GRAPHICAL ABSTRACT



### ARTICLE HISTORY

Received 23 March 2018  
Accepted 1 July 2018

### KEYWORDS

Colloids; dispersions;  
nanoparticles; titanium  
dioxide

## Introduction

Of all the crystalline system of metallic oxide surfaces, titanium oxide (TiO<sub>2</sub>) is the most used. This commodity material has two common crystalline forms, the rutile and the anatase. Titanium dioxide has several applications: it has been used in heterogeneous catalysis, photocatalysis, solar cells for hydrogen and electric power, gas sensors, white pigments, anti-corrosion coatings, optical coatings, ceramics and

electronic devices.<sup>[1, 2]</sup> The surface properties of titanium dioxide promote the application of these particles in photocatalytic processes, which is carried out in aqueous environments. TiO<sub>2</sub> as a pigment is used widely in the paint, papermaking, plastic, cosmetic, and pharmaceutical industries due to its outstanding physicochemical properties, namely, its high refractive index (2.5–2.7 at 599 nm) and low absorption rate; these properties produce a high light scattering that renders materials opaque.<sup>[3]</sup>

## Reflectivity of 1D photonic crystals: A comparison of computational schemes with experimental results

J. S. Pérez-Huerta

*Universidad Autónoma de Zacatecas,  
Unidad Académica de Física,  
Calzada Solidaridad Esquina con Paseo La Bufa S/N,  
Zacatecas, Zac. 98060, México*

D. Ariza-Flores and R. Castro-García\*

*CONACYT-Instituto de investigación en Comunicación Óptica,  
Universidad Autónoma de San Luis Potosí,  
Av. Karakorum 1470, Lomas 4a Sección,  
San Luis Potosí, SLP 78210, México  
|\*ricardo.garcia@uaslp.mx*

W. L. Mochán

*Instituto de Ciencias Físicas,  
Universidad Nacional Autónoma de México,  
Av. Universidad S/N, Col. Chamilpa,  
62210 Cuernavaca, Morelos, México*

G. P. Ortiz

*Departamento de Física,  
Facultad de Ciencias Exactas Naturales y Agrimensura,  
Universidad Nacional del Nordeste,  
Nordeste Av. Libertad 5460, 3400, Corrientes, Argentina*

V. Agarwal

*Centro de Investigación en Ingeniería y Ciencias Aplicadas,  
Universidad del Estado de Morelos,  
Av. Universidad 1001 Col. Chamilpa,  
Cuernavaca, Morelos 62209, México*

Received 7 November 2017

Revised 7 January 2018

Accepted 26 January 2018

Published 28 February 2018

\*Corresponding author.

RESEARCH

Open Access



# Determination of sialic acid in saliva by means of surface-enhanced Raman spectroscopy as a marker in adnexal mass patients: ovarian cancer vs benign cases

José de Jesús Zermeño-Nava<sup>1</sup>, Marco Ulises Martínez-Martínez<sup>1,4</sup>, Ana Laura Ramírez-de-Ávila<sup>1</sup>, Aida Catalina Hernández-Arteaga<sup>2</sup>, Ma. Guadalupe García-Valdivieso<sup>2\*</sup> , Alondra Hernández-Cedillo<sup>2</sup>, Miguel José-Yacamán<sup>2,3</sup> and Hugo Ricardo Navarro-Contreras<sup>2\*</sup>

## Abstract

**Background:** To demonstrate the use of surface-enhanced Raman spectroscopy (SERS) to determine sialic acid (SA) levels in saliva using silver nanoparticles as substrates, in adnexal mass patients scheduled for surgical intervention to remove invasive masses, with the aim to compare SA levels in benign tumor vs ovarian cancer patients.

**Methods:** Quantification of SA levels was accomplished by measuring their SERS and calibrating with analytical reagent SA. The mean SA concentration in saliva from 37 benign adnexal mass resulted smaller (5.1 mg/dL) than the mean concentration in 15 Ovarium cancer patients (23 mg/dL). The cancer condition was determined by biopsy of the removed adnexal mass. The CA-125 biomarker was also measured. The predictive potential of both biomarkers is discussed, together with the malignancy risk index (MRI).

**Results:** Our results showed a sensitivity/specificity of 80%/100% with a cutoff to distinguish between benign/cancer cases of SA 15.5 mg/dL, as established from a ROC analysis. Our results suggest that SA may be a more useful biomarker than CA-125 to detect ovarian cancer.

**Conclusions:** Our results suggest that the SA levels measured from saliva may be as good predictors as the MRI index for the presence of ovarian cancer in sensitivity/negative predictive value and outperforms it in specificity/positive predictive value.

**Keywords:** Sialic Acid, Surface-enhanced Raman, Ag Nanoparticles, Ovarian Cancer

## Background

Ovarian cancer is the seventh most common cancer in women worldwide [1, 2]. In 2012 239,000 ovarian cancer cases were reported; which amounts to 4% of all new cases of cancer in women. Ovarian cancer produced approximately 152,000 deaths in 2012. It is the eighth most common cause of cancer death in women across the world [1, 2].

Ovarian cancer (OC), in general do not produce symptoms at early stages. Additionally, there is no early detection method applicable to the general women population, so the disease is generally advanced when it is diagnosed. Ovarian epithelial cancer is the histological type of major incidence, representing almost 90% of reported cases. In more than 70% of all cases, it is usually detected in the advanced clinical stages III and IV. The 5 year survival rate ranges from approximately 30 to 50% depending on the type of ovarian cancer, being the invasive epithelial ovarian cancer the most common, as well as that of the worst prognosis, in phase III-IV patients, which have a 5–20% five year survival rate [3, 4].

\* Correspondence: [guadalupe.valdivieso@uaslp.mx](mailto:guadalupe.valdivieso@uaslp.mx); [hnavarro@uaslp.mx](mailto:hnavarro@uaslp.mx)

<sup>2</sup>Coordinación para la Innovación y Aplicación de la Ciencia y la Tecnología (CIACYT), Universidad Autónoma de San Luis Potosí, Álvaro Obregón 64, 78000 San Luis Potosí, SLP, Mexico

Full list of author information is available at the end of the article



**Original article:**

**AN AUTOMATED METHOD FOR THE EVALUATION OF BREAST  
CANCER USING INFRARED THERMOGRAPHY**

Antony Morales-Cervantes<sup>1</sup>, Eleazar Samuel Kolosovas-Machuca<sup>2\*</sup>, Edgar Guevara<sup>2,5</sup>,  
Mireya Maruris Reducindo<sup>3</sup>, Alix Berenice Bello Hernández<sup>3</sup>, Manuel Ramos García<sup>4</sup>,  
Francisco Javier González<sup>2</sup>

<sup>1</sup> Facultad de Ciencias, Universidad Autónoma de San Luis Potosí, Av. Dr. Salvador Nava  
Mtz. s/n, Zona Universitaria 78290, San Luis Potosí, SLP, México

<sup>2</sup> Coordinación para la Innovación y la Aplicación de la Ciencia y la Tecnología  
Universidad, Autónoma de San Luis Potosí, Sierra Leona 550, Lomas 2da. Sección 78210,  
San Luis Potosí, SLP, México

<sup>3</sup> Unidad Académica de Ciencias Naturales, Universidad Autónoma de Guerrero, Carretera  
Nal. Chilpancingo-Petaquillas, Ex Rancho Shalako 39105. Petaquillas, Guerrero, México

<sup>4</sup> Hospital General "Dr Raymundo Abarca Alarcón" Chilpancingo, Carretera Federal  
Chilpancingo- Zumpango. Paraje Tierras Prietas S/N, Guerrero, México

<sup>5</sup> CONACYT-Universidad Autónoma de San Luis Potosí, Sierra Leona 550, Lomas 2da.  
Sección 78210, San Luis Potosí, SLP, México

\* Corresponding author: Eleazar Samuel Kolosovas-Machuca, Coordinación para la  
Innovación y la Aplicación de la Ciencia y la Tecnología, Universidad, Autónoma de San  
Luis Potosí, Sierra Leona 550, Lomas 2da. Sección 78210, San Luis Potosí, SLP, México.  
E-mail: [samuel.kolosovas@uaslp.mx](mailto:samuel.kolosovas@uaslp.mx)

<http://dx.doi.org/10.17179/excli2018-1735>

This is an Open Access article distributed under the terms of the Creative Commons Attribution License  
(<http://creativecommons.org/licenses/by/4.0/>).

**ABSTRACT**

Breast cancer is one of the major causes of death for women. Temperature measurement is advantageous because it is non-invasive, non-destructive, and cost-effective. Temperature measurement through infrared thermography is useful to detect changes in blood perfusion that can occur due to inflammation, angiogenesis, or other pathological causes. In this work, we analyzed 206 thermograms of patients with suspected breast cancer, using a classification method, in which thermal asymmetries were computed, the most vascularized areas of each breast were extracted and compared; then these two metrics were added to yield a thermal score, indicative of thermal anomalies. The classification method based on this thermal score allowed us to obtain the test sensitivity of 100 %, specificity of 68.68 %; a positive predictive value of 11.42 % and negative predictive value of 100 %. These results highlight the potential of thermography imaging as adjunctive tool to mammography in breast cancer screening.

**Keywords:** Breast cancer, infrared thermography, automated screening

**INTRODUCTION**

Breast cancer is one of the major causes of death for women (Rastghalam and

Pourghassem, 2016), affecting all social levels of the population. Breast cancer is the most common cancer type in Mexico and



# High and low esterification degree pectins decomposition by hydrolysis and modified Maillard reactions for furfural production

Janneth López-Mercado<sup>1,5</sup> · Apolo Nambo<sup>2</sup> · María-Elena Toribio-Nava<sup>3</sup> · Omar Melgoza-Sevilla<sup>3</sup> · Luis Cázares-Barragán<sup>3</sup> · Leonardo Cajero-Zul<sup>4</sup> · Luis-Guillermo Guerrero-Ramírez<sup>4</sup> · Brent E. Handy<sup>5</sup> · Maria-Guadalupe Cardenas-Galindo<sup>5</sup>

Received: 9 May 2017 / Accepted: 25 June 2018 / Published online: 3 July 2018  
© Springer-Verlag GmbH Germany, part of Springer Nature 2018

## Abstract

In recent years, there has been a great interest in the conversion of lignocellulosic structures to furfural. There are many technologies available for this process. Nonetheless, the present work reports for the first time the use of pectin, a non-lignocellulosic structure, for furfural production. The pectin was extracted from food industry waste derived from cactuses, orange peels and mangoes peels. The extracted pectins were analyzed by infrared spectroscopy (ATR–FTIR) in order to evaluate the degree of esterification (DE). The high DE influences in the hydrolysis reaction in the following stages: (1) hydration, it allows a fast glycosidic bond cleavage in the polysaccharide. (2) Dehydration, an intermediary step in the furfural production from galacturonic acid. The Maillard reaction herein reported not only is used in a novel way to produce furfural but also it has been modified to be performed in acidic conditions to increase the furfural production rate. From the evaluated reactions, it was found that the highest furfural production was obtained with manila mango pectin (82.6 g/L) with a DE of 51.2%. These findings demonstrate that pectins with DE below 75%, the minimum value to be considered for applications in the food and pharmaceutical industries, could be applied for the generation of furfural, a chemical platform for the production of chemicals and biofuels.

**Keywords** Pectin decomposition · Degree of esterification · Acid reaction · Maillard reaction · Furfural

**Electronic supplementary material** The online version of this article (<https://doi.org/10.1007/s10098-018-1570-y>) contains supplementary material, which is available to authorized users.

✉ Janneth López-Mercado  
jannlopezm@gmail.com

<sup>1</sup> Ingeniería en Energía, Universidad de la Ciénega del Estado de Michoacán, Lomas de la Universidad, Avenida Universidad No 3000, C.P. 59103 Sahuayo, Michoacán, Mexico

<sup>2</sup> Conn Center for Renewable Energy Research, University of Louisville, 40292 Louisville, KY, USA

<sup>3</sup> Departamento de Ingeniería de Industrias Alimentarias, Instituto Tecnológico de Estudios Superiores de Zamora, Km 7 carretera Zamora-La Piedad S/N, Col. El Sauz de Abajo, C.P. 59720 Zamora, Michoacán, Mexico

<sup>4</sup> Centro Universitario de Ciencias Exactas e Ingenierías, Universidad de Guadalajara, Blvd. Marcelino García Barragán No 1421, C.P. 44430 Guadalajara, Jalisco, Mexico

<sup>5</sup> Facultad de Ciencias Químicas, Universidad Autónoma de San Luis Potosí, Av. Dr. Manuel Nava No. 6, C.P. 78210 San Luis Potosí, SLP, Mexico

## Abbreviations

DE	Degree of esterification
GalA.	Galacturonic acid
K.P.	Kent mango peels pectin
M.P.	Manila mango peels pectin
C.P.	Cactus pectin
O.P.	Orange peels pectin
A.P.	Apple pectin
RH.	Relative humidity

## Introduction

Since 2015, Michoacán in the “El Bajío” region of México has been the primary exporter of mango, orange, bananas, berries, limes, etc., according to Secretaría de Agricultura, Ganadería, Desarrollo Rural, Pesca y Alimentación (SAGARPA) [SAGARPA 2015, SAGARPA 2016]. Many of these fruits are processed into purées, fruit base for ice cream, yogurt, baby food, jams, fillings, syrups or simply frozen cubes. These processes generate wastes and



## Full Length Article

# On the origin of reflectance-anisotropy oscillations during GaAs (001) homoepitaxy

J. Ortega-Gallegos<sup>a,\*</sup>, L.E. Guevara-Macías<sup>a</sup>, A.D. Ariza-Flores<sup>a,b</sup>, R. Castro-García<sup>a,b</sup>, L.F. Lastras-Martínez<sup>a</sup>, R.E. Balderas-Navarro<sup>a</sup>, R.E. López-Estopier<sup>a,b</sup>, A. Lastras-Martínez<sup>a</sup>

<sup>a</sup> Instituto de Investigación en Comunicación Óptica, Universidad Autónoma de San Luis Potosí, Alvaro Obregón 64, San Luis Potosí, SLP 78000, Mexico

<sup>b</sup> CONACyT - Instituto de Investigación en Comunicación Óptica, Universidad Autónoma de San Luis Potosí, Alvaro Obregón 64, San Luis Potosí, SLP 78000, Mexico

## ARTICLE INFO

## Article history:

Received 25 October 2017

Revised 22 December 2017

Accepted 28 December 2017

Available online 6 January 2018

## Keywords:

Reflectance anisotropy oscillations

Real-time measurements

GaAs homoepitaxy

## ABSTRACT

We report on the first spectroscopic study of reflectance-anisotropy (RA) oscillations during molecular beam epitaxy (MBE) GaAs homoepitaxy. Real-time RA spectra measured during epitaxial growth were carried out with a recently developed rapid RA multichannel spectrometer with 100 ms per spectrum acquisition time. An analysis of the time-resolved RA spectra shows that RA oscillations are mostly due to the periodic modulation of the surface orthorhombic strain associated to surface reconstruction. Results reported here demonstrate the power of real-time RA spectroscopy as a probe for the study of epitaxial growth processes. In particular, given its sub monolayer surface-strain sensitivity, RA spectroscopy results a very convenient tool to study epitaxial growth mechanisms in real-time with sub monolayer resolution. This capability allows for real-time RA spectroscopy to be used as a probe for the *in situ*, real-time control of epitaxial growth, with the additional advantage of operating in higher pressure systems such as CVD, where RHEED monitoring cannot be implemented.

© 2018 Elsevier B.V. All rights reserved.

## 1. Introduction

The fabrication of advanced optoelectronic devices based on zincblende semiconductors demands for probes with both real-time monitoring and feedback control capabilities for the epitaxial growth process with at least monolayer (ML) resolution. Optical probes would be advantageous for this application given their instrumental simplicity and provided we overcome their intrinsic low surface specificity. Reflectance anisotropy (RA) is an optical polarization contrast technique which enhances the surface-related response by taking advantage of the reduced symmetry of the surface or near surface region of the crystal. RA measures the difference in the optical reflectivity between two principal axis of the crystal, thus suppressing the polarization-independent bulk signal and enhancing the surface response [1].

RA has been applied to study the kinetics of the epitaxial growth of various zincblende semiconductors, demonstrating high sensitivity to the different stages of the growth process [2,3]. In particular, it is known that the intensity of the RA signal oscillates during growth with the same oscillation period as that of specular

RHEED oscillations [4], which is known to correspond to the time necessary to grow one monolayer. RHEED oscillations are widely accepted to be associated to periodic changes in surface micro roughness that take place during layer-by-layer growth [5]. Phenomena leading to RA oscillations, in contrast, are not fully understood. In this regards, on the basis of an effective medium model, Aspnes argues that optical anisotropies associated to surface roughness are too small to explain experimental results and concludes that they have a surface chemistry origin [6]. RA oscillations have also been explained on the basis of a modulation of As dimer coverage during growth as dimers are preferentially broken at island edges [7].

Previous determinations of RA oscillations have been carried out at a single-wavelength or at most a few wavelengths [3,4,7]. However, as it has been shown elsewhere, RA signals may comprise more than one independent component [8,9], hence hampering the physical interpretation of RA oscillations on the basis of single-wavelength data. A deeper understanding of RA oscillations thus demands time-resolved spectroscopic measurements. Carrying out such measurements, nevertheless, demand a rapid RA spectrometer, fast enough to follow in real-time the kinetics of epitaxial growth of III-V compounds (spectrum acquisition times of the order of 0.1 s and  $\Delta R/R$  amplitude in the range  $10^{-3}$ ). Harrison et al., developed a 16 channel rapid RA spectrometer to study the

\* Corresponding author.

E-mail addresses: [jortega@cactus.iico.uaslp.mx](mailto:jortega@cactus.iico.uaslp.mx) (J. Ortega-Gallegos), [alastras@gmail.com](mailto:alastras@gmail.com) (A. Lastras-Martínez).

# Dirac Equation and Optical Wave Propagation in One Dimension

Gabriel González\*

**We show that the propagation of transverse electric (TE) polarized waves in one-dimensional inhomogeneous settings can be written in the form of the Dirac equation in one space dimension with a Lorentz scalar potential, and consequently perform photonic simulations of the Dirac equation in optical structures. In particular, we propose how the zero energy state of the Jackiw–Rebbi model can be generated in an optical set-up by controlling the refractive index landscape, where TE-polarized waves mimic the Dirac particles and the soliton field can be tuned by adjusting the refractive index.**

The Dirac equation<sup>[1]</sup> plays a key role to many exotic physical phenomena such as graphene,<sup>[2]</sup> topological insulators<sup>[3]</sup> and superconductors.<sup>[4]</sup> These systems proved to be ideal testing grounds for theories of the coexistence of quantum and relativistic effects in condensed matter physics. A very interesting result emerging from the Dirac equation is given by the Jackiw–Rebbi (JR) model which predicts the existence of zero energy states when the Dirac mass changes sign.<sup>[5]</sup> The JR model describes a one dimensional Dirac field coupled to a static background soliton field and is known as one of the earliest theoretical description of a topological insulator where the zero energy mode can be understood as the edge state. The Jackiw–Rebbi model can be equivalently thought of as the model describing a massless Dirac particle under a Lorentz scalar potential. In particular, the Jackiw–Rebbi model has been studied by Su, Shrieffer and Heeger in the continuum limit of polyacetylene.<sup>[6]</sup> Since the derivation of the JR model many important and useful variations of the model have been investigated such as the Rajaraman–Bell model for a finite volume,<sup>[8]</sup> the massive Jackiw–Rebbi model,<sup>[9]</sup> the coupled fermion–kink model<sup>[10]</sup> and the Jackiw–Rebbi model in distinct kinklike backgrounds.<sup>[11]</sup>

Many experimental proposals have been made to experimentally detect the zero energy states of the JR model using different

physical platforms such as optical structures,<sup>[7,12–15]</sup> metamaterials,<sup>[16]</sup> ion traps<sup>[17]</sup> and in a silicon platform.<sup>[18]</sup> Recently, the photonic topological zero energy state were experimentally observed in binary waveguide arrays,<sup>[19,20]</sup> and more recently in a non-Hermitian system involving loss<sup>[21]</sup> and in the context of graphene ribbons.<sup>[22]</sup> Localized zero energy states are of topological origin and from a quantum information perspective these states are very robust against environmental effects which is


advantageous when using these states to encode quantum information for quantum memory. It is currently debated whether topological zero energy states can exist at all in  $\mathcal{PT}$  symmetric systems.

The purpose of this letter is to optically simulate the zero energy state of a relativistic quantum system, the Jackiw–Rebbi model, by means of optical wave propagation in one dimensional inhomogeneous media. In particular, we demonstrate that the TE-polarized electromagnetic waves in one dimensional inhomogeneous media can be mapped into the Dirac equation in one dimension with a Lorentz scalar potential. The duality between classical optical wave propagation and relativistic quantum mechanics in one dimension provides a way to explore the JR model using a macroscopic optical setting by tailoring the refractive index in an optical structure and visualize with classical optics the dynamical aspects of relativistic quantum phenomena. The duality relates the refractive index with the Lorentz scalar potential of the Dirac equation and the TE-electric mode with the wave function. We also show that the JR model can be described by a non-Hermitian Dirac Hamiltonian by using a complex Dirac mass and propose the corresponding refractive index for such non-Hermitian  $\mathcal{PT}$  symmetric system. It is of great interest to see whether topological protection can survive in the presence of gain and loss optical waveguides. Remarkably, as shown here for the complex JR model such robustness persists even though the spatially distributed gain and loss renders a non-Hermitian Hamiltonian and breaks the time reversal symmetry of the system. Therefore, our results provide two different ways for directly realizing the zero energy state of the JR model, one which corresponds to an Hermitian system and another which corresponds to a non-Hermitian system with  $\mathcal{PT}$  symmetry.

To explore the connection between the Dirac equation and optical wave propagation in one dimension with an arbitrary refractive index distribution  $n(x)$  we consider TE waves propagating in the  $xz$  plane. Field modes propagating in this system are described by the following Helmholtz equation<sup>[23,24]</sup>

Dr. G. González  
Cátedras CONACYT  
Universidad Autónoma de San Luis Potosí  
San Luis Potosí 78000, Mexico  
E-mail: gabriel.gonzalez@uaslp.mx

Dr. G. González  
Coordinación para la Innovación y la Aplicación de la Ciencia y la Tecnología  
Universidad Autónoma de San Luis Potosí  
San Luis Potosí 78000, Mexico

 The ORCID identification number(s) for the author(s) of this article can be found under <https://doi.org/10.1002/pssr.201700357>.

DOI: 10.1002/pssr.201700357



# Resistive random-access memory based on ratioed memristors

Miguel Angel Lastras-Montaña<sup>1\*</sup> and Kwang-Ting Cheng<sup>2\*</sup>

**Resistive random-access memories made from memristor crossbar arrays could provide the next generation of non-volatile memories. However, integrating large memristor crossbar arrays is challenging due to the high power consumption that originates from leakage currents (known as the sneak-path problem) and the large device-to-device and cycle-to-cycle variations of memristors. Here we report a memory cell comprised of two serially connected memristors and a minimum-sized transistor. With this approach, we use the ratio of the resistances of the memristors to encode information, rather than the absolute resistance of a single memristor, as is traditionally used in resistive-based memories. The minimum-sized transistor, which is connected to the midpoint between the two series-connected memristors, is used to sense the voltage to read the state of the cell and to assist with write operations. Our memory cell design solves the sneak-path problem and, compared to the traditional resistance-based current sensing approach for memory reads, our ratio-based voltage sensing scheme is more robust and less prone to data errors caused by variations in memristors.**

Resistive random-access memory (ReRAM) based on two-terminal resistance-switching memristive devices is a promising candidate to fill the gap between the main working memory and the storage in modern computing systems. ReRAM, a non-volatile memory (NVM) technology, offers memory densities that are comparable to those of NAND flash, the leading NVM storage technology, and fast random accesses that are comparable to those of dynamic random-access memory, the de facto standard for main working memory<sup>1</sup>. ReRAM, therefore, effectively offers the advantages of both technologies. Three key attributes make memristor-based ReRAM attractive compared to other NVM technologies. First, shrinking the size of the two electrodes of the memristor will not degrade its key properties, such as retention, switching time and on/off ratio, as these properties are mainly determined by a single localized nanometre-scale filament. Second, the memristor's nonlinear switching dynamics allows removal of the access element (for example, a transistor) from the memory cell, which is beneficial in reducing the cell's complexity and size, as the access element usually dominates its overall size. Third, a memristor has a simple metal–insulator–metal structure. The second and third attributes enable memristive devices to be organized into a high-density crossbar array. However, these same three attributes are also the sources of its biggest limitations: its filamentary nature leads to large device-to-device and cycle-to-cycle variations and the use of a crossbar array results in the sneak-path problem.

In this Article, we report a ReRAM cell design and an information encoding scheme that together solve the sneak-path problem and greatly improve the tolerance of ReRAM to memristor variations. The memory cell, which is termed an H3 cell, consists of two memristors and a minimum-sized transistor. We use the ratio of the resistances of the two memristors in an H3 cell to encode information, in contrast to the existing ReRAM architecture's reliance on a single memristor's absolute resistance to encode information. This results in much greater data reliability in the presence of sources of variation in memristors. Furthermore, our solution is complementary to any device- and material-based solution. The proposed

cell design and architecture can substantially enhance the benefits of any device-level improvement.

## Memristive devices and ReRAM architectures

The fingerprint of a bipolar memristor is a pinched hysteresis loop in the current–voltage ( $I$ – $V$ ) plane<sup>2</sup>, as shown in Fig. 1a for a titanium oxide-based device. Physically, a memristor is a two-terminal device formed by two metallic electrodes sandwiching a thin layer of insulating material, as illustrated in Fig. 1b. As fabricated, a memristor typically presents a very high resistance across its terminals (an unformed state) and an initial one-time electroforming step is needed. This is done by applying a voltage or current sweep across the device's terminals until a soft breakdown of the thin insulating layer occurs, creating a conductive filament that brings the memristor into a low-resistance state (LRS)<sup>3</sup>. Changing the memristor from an LRS to a high-resistance state (HRS) requires a 'reset' operation, in which a voltage greater than a reset threshold  $V_{\text{RESET}}$  is applied to partially destroy the conductive filament. The process of changing the memristor from an HRS to an LRS, called a set operation, involves applying a voltage greater than a set threshold  $V_{\text{SET}}$  to create the conductive filament again. The main memory element in a ReRAM unit cell is the memristor. Logic '1' is written into a cell by setting its memristor to an LRS. Logic '0' is written by resetting it to an HRS. The state of a memory cell is typically determined by applying a small voltage across its memristor and comparing the resulting current against a reference current. We call this a 'resistance-based current sensing' approach.

The crossbar architecture, illustrated in Fig. 1c, is the preferred ReRAM architecture from the density point of view. This is also known as the  $1TnR$  architecture, as every electrode is connected to  $n$  memristors and one transistor is needed to access each electrode when reading from or writing to any of the  $n$  memristors. This architecture can achieve the smallest theoretical memory cell size,  $4F^2$ , when both the electrodes and the spaces between them are of width  $F$ . Writing to a device is typically done using the 'V/3' biasing scheme<sup>4</sup>, in which the required write voltage

<sup>1</sup>Electrical and Computer Engineering Department, University of California Santa Barbara, Santa Barbara, CA, USA. <sup>2</sup>School of Engineering, Hong Kong University of Science and Technology, Clear Water Bay, Kowloon, Hong Kong. \*e-mail: [mllastras@ece.ucsb.edu](mailto:mllastras@ece.ucsb.edu); [timcheng@ust.hk](mailto:timcheng@ust.hk)

# Rapid Reflectance-Anisotropy Spectroscopy as an Optical Probe for Real-Time Monitoring of Thin Film Deposition

J. Ortega-Gallegos<sup>1,a)</sup>, L. E. Guevara-Macías<sup>1</sup>, A. Lastras-Martínez<sup>1</sup>, D. Ariza-Flores<sup>2</sup>, R.E. Balderas-Navarro<sup>1</sup> and L.F. Lastras-Martínez<sup>1</sup>

<sup>1</sup>*Instituto de Investigación en Comunicación Óptica, Universidad Autónoma de San Luis Potosí, Alvaro Obregón 64, San Luis Potosí, SLP 78000, México Phone: 52 (444) 825 0183, Fax: 52 (444) 825 0198.*

<sup>2</sup>*Cátedras Conacyt, Av. Insurgentes 1582, Crédito Constructor, Delegación Benito Juárez, CDMX 03940, México.*

<sup>a)</sup>Corresponding author: jortega@cactus.iico.uaslp.mx

**Abstract.** We report on real-time spectroscopic reflectance anisotropy measurements carried out during the epitaxial growth of GaAs/GaAs (001). Our work is aimed to the study of fundamental processes occurring during the epitaxial growth of III-V semiconductors. We show that during growth there is an oscillation in the surface strain associated to surface reconstruction, suggesting the existence of a mechanism of periodic build up-relaxation of the surface strain, indicating that the technique employed in this work may potentially distinguish between two reconstruction phases.

## INTRODUCTION

The growth of well controlled surface templates with III-V epitaxy remains a challenge and is a very interesting topic due to their potential applications for nanoscale devices based on GaAs [1, 2]. For this purpose, non-invasive diagnostic probes such as Reflectance-Anisotropy Spectroscopy (RAS) would be of great value. The use of this probe in a feedback control loop would allow for the precise control of surface reconstruction during the for molecular beam epitaxy (MBE) growth. In this regards, it is known that there is close relationship between RAS line shape and surface reconstruction. In the case of the GaAs(001) surface, RAS has proved to be highly sensitive to surface reconstruction, giving information on three types of As-stabilized reconstructions, namely  $\alpha(2 \times 4)$ ,  $\beta(2 \times 4)$  and  $\gamma(2 \times 4)$  [3], and  $\alpha c(4 \times 4)$  and  $\beta c(4 \times 4)$  [4]. It has been reported that RA spectra around  $E_1$  and  $E_1 + \Delta_1$  transitions comprise several components. Among them, we include components induced by surface roughness [5] and surface anisotropic strain fields for both  $c(4 \times 4)$  [6] and  $(2 \times 4)$  surface reconstructions [7]. Such strains are related to a surface stress arising from charge redistribution in the surface bonds due to the absence of atoms above the surface [8]. Reconstruction-induced strain has an orthorhombic symmetry and may penetrates into a region 20 nm thick [6].

Recently, we have shown that it is possible to use real-time RA spectroscopy for monitoring processes taking place during the homoepitaxial growth of GaAs/GaAs (001) [9]. In this paper we report on a real-time RAS investigation of the dynamics of homoepitaxial MBE growth of GaAs (001) at a temperature of 520 °C. Particularly, we focus on the study of RA amplitude oscillations that are linked to the layer by layer growth model. We note that the growth temperature employed in this work is one of the standards in the manufacture of thin films for optoelectronic device applications.

## EXPERIMENTAL DETAILS

Undoped GaAs films were grown on GaAs (001) substrates in a solid source molecular beam epitaxy system (Riber 32P). A home made rapid RA spectrometer attached to the growth chamber enables the acquisition of RA spectra at a rate of 10 spectra/s [10]. The setup allows for the simultaneous measurement of RA spectra and Reflection High Energy Electron Diffraction (RHEED) oscillations during growth. To remove the surface native oxide the GaAs substrate was heated to at a temperature 600 °C until a  $(2 \times 4)$  RHEED pattern was observed. An undoped 0.3  $\mu\text{m}$  thick buffer

# Real-time Optical Monitoring of Semiconductor Epitaxial Growth

A. Lastras-Martínez<sup>1,a)</sup>, J. Ortega-Gallegos<sup>1</sup>, L.E. Guevara-Macías<sup>1</sup>, D. Ariza-Flores<sup>2</sup>, O. Núñez-Olvera<sup>1</sup>, R.E. López-Estopier<sup>2</sup>, R.E. Balderas-Navarro<sup>1</sup> and L.F. Lastras-Martínez<sup>1</sup>

<sup>1</sup> *Instituto de Investigación en Comunicación Óptica, Universidad Autónoma de San Luis Potosí, San Luis Potosí, México.*

<sup>2</sup> *Cátedras Conacyt, Av. Insurgentes 1582, Crédito Constructor, Delegación Benito Juárez, CDMX 03940, México.*

<sup>a)</sup>Corresponding author: [alastras@gmail.com](mailto:alastras@gmail.com)

**Abstract.** We report on time-resolved Reflectance Anisotropy Spectroscopy (RAS) measurements carried out during the molecular beam epitaxial growth of GaAs (001). Growth started on a c(4x4) reconstructed surface which changed to (2x4) and then to (4x) as growth progressed. We found that reflectance anisotropy spectra comprise three components, each one with a specific physical origin and determine their time evolution as a function of epitaxil film thickness. We conclude that RAS is a powerful probe for the monitoring and potentially for the control of epitaxial growth.

## INTRODUCTION

Light probes, being non-invasive, result very attractive tools for the real-time monitoring of the epitaxial growth of semiconductors. Depending on photon energy, however, light impinging on the substrate penetrates to a depth of 50-500 monolayer, thus limiting surface sensitivity. More than two decades ago, D.E. Aspnes introduced Reflectance-anisotropy spectroscopy (RAS) (also known as Reflectance-difference spectroscopy) which overcomes this limitation by measuring the difference in reflectivity for two mutually orthogonal polarizations [1]. In the past, however, despite the demonstrated RAS surface sensitivity, its use for epitaxial growth monitoring has been hindered by 1) the lack of reflectance anisotropy (RA) spectrometers fast enough to follow atomic processes during growth and 2) the limited understanding of the physics underlining the optical anisotropy of semiconductor surfaces. Here we address these two points and report on time-resolved RAS measurements carried out during the MBE homoepitaxial growth of GaAs (001) that show RAS to be a powerful probe for the monitoring and control of epitaxial growth.

## EXPERIMENTAL

Epitaxial growth was carried out on GaAs (001) substrates in a solid source molecular beam epitaxy chamber (Riber 32P). Growth temperature and As<sub>4</sub> overpressure were set to 520 °C and 2x10<sup>-6</sup> Torr, respectively. With these conditions, during the first growth stage the GaAs film growth rate was 0.19 ML/s, decreasing to 0.13 ML/s as growth stabilized. Prior to RA measurements a 0.2 μm thick undoped GaAs buffer layer was grown on the GaAs substrate. The sample surface is kept under As<sub>4</sub> flux along the whole experiment. Growth is started upon opening the Ga shutter on a c(4x4) reconstructed surface which first changes to (2x4) and then to a Ga-rich reconstruction. As discussed below, the RA spectrum line shape changes substantially along growth.



# Optimizing the oxidation level of PEDOT anode in air-PEDOT battery

Marisol Reyes-Reyes<sup>a,\*</sup>, Román López-Sandoval<sup>b</sup>

<sup>a</sup> Instituto de Investigación en Comunicación Óptica, Universidad Autónoma de San Luis Potosí, Álvaro Obregón 64, San Luis Potosí 78000, Mexico

<sup>b</sup> Advanced Materials Department, IPICYT, Camino a la Presa San José 2055, Col. Lomas 4a Sección, San Luis Potosí 78216, Mexico

## ARTICLE INFO

### Keywords:

PEDOT:PSS  
Conducting polymer  
Polymer battery  
Air stable  
DBU  
DMSO

## ABSTRACT

We report an air-PEDOT battery where an optimized oxidation level of the PEDOT anode was performed using a simple dedoping process, resulting in batteries with high stability in air. Some PEDOT:PSS chains were reduced to their neutral state, preserving their good electrical conductivity, by dipping the PEDOT:PSS films into mixtures of 1,8-diazabicyclo[5.4.0]undec-7-ene (DBU) and dimethyl sulfoxide (DMSO). Because of the neutral PEDOT chains are susceptible to being reoxidized in air, polyethyleneimine (PEI) was coated on these DMSO-DBU/PEDOT:PSS anodes to ensure their air stability and to maintain their low level of oxidation during the battery operation. The difference in the oxidation level between the dedoped PEDOT:PSS and pristine PEDOT:PSS electrodes produces an open circuit voltage of about 0.80 V almost constant by several days (around 30 days) in air. These batteries present discharge currents of  $\approx 2 \mu\text{A}$  with an electrical load of  $0.1 \text{ M}\Omega$  during 10 h of operation, output powers of  $\approx 1.2 \mu\text{W}$ , using an electrical load of  $265 \text{ k}\Omega$ , which is in the required range for powering wireless transceiver and sensors.

## 1. Introduction

Polymers have a great number of interesting properties such as good tenacity, good elongation, ease of processing, low weight, and low cost that makes them exceptional for their applications in organic electronics. The excellent conductivity of conjugated polymers opens up new design possibilities in the fields of production, storage and transformation of electrical energy. Additionally, polymer-based devices could be more economical and less polluting, compared with those based in inorganic semiconductors, and a promising technology for flexible electronics. However, the conductive polymers present two main disadvantages for a possible technological application: their insolubility associated to their low processability and their conductivity instability given by their degradation in air. Poly(3,4-ethylenedioxythiophene) doped with the polymeric counteranion poly(styrenesulfonate) (PEDOT:PSS) can be an attractive alternative because of its oxidized state (*p*-doped) (PEDOT<sup>+</sup>) presents good electrical conductivity, very high electrochemical stability, good air stability and is easy-to-process due to the PSS counterion. The PSS counterion acts as the source for the charge balancing [1,2] and keeps the PEDOT chains dispersed in the aqueous medium. Moreover, some reports show that PEDOT chains can be carried up to a partial reduced state (dedoped, neutral, PEDOT<sup>0</sup>) by using reducing agents [3–8] resulting in changes in their electrical, thermoelectric, and optical properties [5–9], opening perspectives for new applications.

Between the possible applications of PEDOT:PSS in organic electronics, one of the most interesting is their use in organic batteries. In fact, PEDOT has already been used as cathode in metal/air batteries [10,11] and all polymer-air batteries in coplanar configuration have been fabricated with a polyethyleneimine (PEI)/PEDOT:PSS electrode as anode, PEDOT:PSS electrode as cathode and PSSNa as electrolyte. In this last case, it was reported an initial open circuit voltage ( $V_{OC}$ ) of  $\sim 0.53 \text{ V}$  that drops to  $0.48 \text{ V}$  during the first 50 h of self-discharge in air. In addition, these batteries showed an output power of  $0.67 \mu\text{W}$  using a  $265 \text{ k}\Omega$  electrical load, and an electrical discharge current of  $1.7 \mu\text{A}$  during 1 h, using a load of  $0.1 \text{ M}\Omega$  [7]. The same type of batteries, but in the stacked configuration, was fabricated with the aim of increasing battery capacity, using a screen printing fabrication route that will facilitate large scale manufacturing. These last batteries give a  $V_{OC}$  of  $\sim 0.60 \text{ V}$ , displayed a practical specific capacity of  $5.5 \text{ mAhg}^{-1}$  and an electrical discharge current of  $0.6 \mu\text{A}$  [12]. In all polymer air batteries based in PEDOT:PSS, the use of PEI on the anode is a key factor for the battery operation. PEI has a basic character, reduces the oxidized PEDOT<sup>+</sup> to its neutral state PEDOT<sup>0</sup> and keeps this neutral state stable in air through dynamic redox reactions [7]. Even though the electrical current and output power of these all polymer air-PEDOT batteries are very small, they could be used in niche market such as in  $10 \mu\text{W}$  low power RFID chips, in  $17 \mu\text{W}$  at  $1.4\text{--}1.6 \text{ V}$  operational amplifier, in  $20 \mu\text{W}$  at  $0.9 \text{ V}$  GMR-switch or for the update of a  $5 \mu\text{W cm}^{-2}$  e-ink display [13].

\* Corresponding author.

E-mail addresses: [reyesm@iico.uaslp.mx](mailto:reyesm@iico.uaslp.mx) (M. Reyes-Reyes), [sandov@ipicyt.edu.mx](mailto:sandov@ipicyt.edu.mx) (R. López-Sandoval).



## Tuning the dedoping process of PEDOT:PSS films using DBU-solvent complexes

Marisol Reyes-Reyes<sup>a,\*</sup>, Román López-Sandoval<sup>b</sup>, Eduardo Tovar-Martínez<sup>b</sup>,  
Jorge V. Cabrera-Salazar<sup>b</sup>, Geminiano Martínez-Ponce<sup>c</sup>

<sup>a</sup> Instituto de Investigación en Comunicación Óptica, Universidad Autónoma de San Luis Potosí, Álvaro Obregón 64, San Luis Potosí 78000, Mexico

<sup>b</sup> Advanced Materials Department, IPICYT, Camino a la Presa San José 2055, Col. Lomas 4a Sección, San Luis Potosí 78216, Mexico

<sup>c</sup> Centro de Investigaciones en Óptica, Apdo. Postal 1-948, 37000 León, Guanajuato, Mexico

### ARTICLE INFO

#### Keywords:

PEDOT:PSS  
Dedoping  
DBU complexes  
Basicity  
Protonation

#### Abstract

In this study, we report a successful simple technique to dedope pristine PEDOT:PSS films at room temperature by dipping the films into 1,8-diazabicyclo[5.4.0]undec-7-ene (DBU) mixes with different solvents such as dimethyl sulfoxide (DMSO), acetonitrile (MeCN) and deionized (DI) water. The treated PEDOT:PSS films presented a strong  $\pi$ - $\pi^*$  absorption band centered at 630 nm, which indicated that the PEDOT chains were being reduced to their neutral state. The dedoping efficiency of the PEDOT chains depended on the used DBU complex, the DBU concentration in the mixture as well as the immersion time, which was quantified comparing the relative intensities between the  $\pi$ - $\pi^*$  and the polaronic (centered around 900 nm) bands. The best dedoping efficiencies of PEDOT:PSS films were obtained using MeCN/DBU or DI water/DBU complexes, as the polaronic band almost disappeared, whereas using DMSO/DBU complex the polaronic band was always present. This difference was mainly related to the degree of basicity of the DBU complexes and solubility extent of PEDOT:PSS in the various solvents. Finally, thick dedoped PEDOT:PSS films showed a strong yellow emission when they were excited with a 488 nm laser. The encapsulated dedoped thick films endured up to 50 mW of laser power without impacting their luminescent and physical properties.

### 1. Introduction

Conjugated organic polymers have attracted great interest because of their potential applications in corrosion resistance coatings [1],

electromagnetic shielding [2] and development of organic electronic devices [3–8]. In particular, the polymer poly(3,4-ethylenedioxythiophene) doped with the polymeric counteranion poly(styrenesulfonate) (PEDOT:PSS) has acquired high relevance owing to the various and increasing uses that include for photographic films, electrochromic devices [9], organic field effect transistors [10], light emitting diodes [11] and photovoltaic cells [12]. The particular properties in the oxidized state of PEDOT [13], as well as its very high electrochemical stability and easy-to-process, are due to the PSS counterion that acts as the source for the charge balancing [14,15] and keeps the PEDOT segments dispersed in the aqueous medium. The oxidized state (*p*-doped) of PEDOT is one of the most studied; in contrast, although significant efforts were devoted to obtain dedoped (reduced, neutral) PEDOT segments, this has been scantily investigated. Some reports show that PEDOT:PSS can be dedoped by using reducing agents [16–19] resulting in changes in the electrical, thermoelectric, and optical properties [16–20]. In particular, one of the possible applications, of dedoped PEDOT in organic electronics, is their use in organic batteries as anode [17,21]. Previously, we reported a partial reduction of PEDOT:PSS to its neutral state by a simple process consisting in the addition of 1,8-diazabicyclo[5.4.0]undec-7-ene (DBU, C<sub>9</sub>H<sub>16</sub>N<sub>2</sub>) to the aqueous PEDOT:PSS dispersion. In addition, these dedoped samples in aqueous dispersion as well as encapsulated films showed a strong yellow emission using a 10 mW laser power [22].

In the present work, we have prepared a series of DBU complexes, i.e. DBU was mixed with different solvents in order to create a

\* Corresponding author.

E-mail address: [reyesm@iico.uaslp.mx](mailto:reyesm@iico.uaslp.mx) (M. Reyes-Reyes).



# Adsorption study of xanthates on $\text{PbSO}_4$ by titration microcalorimetry

A. Robledo-Cabrera<sup>1</sup> · A. López-Valdivieso<sup>1</sup> · J. E. Pérez-López<sup>2</sup> · O. A. Orozco-Navarro<sup>1</sup>

Received: 25 November 2017 / Accepted: 4 March 2018 / Published online: 12 March 2018

© Akadémiai Kiadó, Budapest, Hungary 2018

## Abstract

Isoperibol (pseudo-adiabatic) titration microcalorimetry was used to study the adsorption of various xanthates  $[\text{CH}_3(\text{CH}_2)_n\text{OCS}_2^-]$  at the  $\text{PbSO}_4$ /aqueous solution interface. The effect of the xanthate alkyl chain length (1n–3n) on the adsorption heat was evaluated. Xanthate adsorption isotherms were also determined. Furthermore, the amount of  $\text{SO}_4$  into the aqueous solution was quantified to correlate it with the xanthate uptake by  $\text{PbSO}_4$ . The adsorption isotherms and the adsorption heat of the xanthates showed two steps. The first step occurred within a sub-monolayer xanthate coverage and was attributed to chemisorption of the xanthates exchanging surface hydroxyls to form  $\text{CH}_3(\text{CH}_2)_n\text{OCS}_2\text{Pb}$ . Lead xanthate  $(\text{CH}_3(\text{CH}_2)_n\text{OCS}_2)_2\text{Pb}$  multilayers formed in the second step, which was attributed to an ionic exchange chemical reaction between the xanthates and  $\text{PbSO}_4(\text{aq})$ . In the chemisorption step, the heat was found to be independent of the xanthate alkyl chain length and to linearly decrease in magnitude with the xanthate adsorption. In the multilayer formation step, the magnitude of the integral heat increased with the chain length of the xanthate. Heat contributions due to both the alkyl chain length and the interaction between the xanthate polar group and  $\text{PbSO}_4(\text{aq})$  for the formation of lead xanthates are presented. Raman spectroscopy was used to characterize the lead xanthate multilayers on  $\text{PbSO}_4$ .

**Keywords** Microcalorimetry · Xanthates · Flotation · Adsorption · Lead sulfate · Raman spectroscopy

## Introduction

Xanthates are hetero-polar chemical reagents,  $\text{CH}_3(\text{CH}_2)_n\text{OCS}_2^-$ , which are used to concentrate base-metal sulfide minerals like galena ( $\text{PbS}$ ), sphalerite ( $\text{ZnS}$ ), chalcopyrite ( $\text{CuFeS}_2$ ), and so on, by the flotation process. In this process, it is of great interest to understand the adsorption mechanisms of the xanthates on the sulfides. Various techniques have been used to study the adsorption mechanisms, namely adsorption, electrokinetics, contact angle measurements, microcalorimetry, IR spectroscopy, electrochemical methods and XPS-voltammetry [1–5]. Of all of them, the titration microcalorimetry technique has been seldom used despite the fact that it has the advantage of determining the heat involved in the adsorption process.

Knowing this heat and the resulting surface species would lead to a comprehensive understanding of the nature of the interaction between the xanthates and the sulfide surface. Microcalorimetry has been used to determine the enthalpy of formation and solubility product of lead xanthates [15], to correlate the adsorption heat of xanthates with the floatability of  $\text{PbS}$  looking at the effect of metal impurities (Ag, Bi, Zn, Sb, Mn and Cu) in the  $\text{PbS}$  [23], and to correlate the adsorption heat of xanthates of various chain lengths with the floatability of  $\text{CuFeS}_2$ , pyrite ( $\text{FeS}_2$ ) and pyrrhotite ( $\text{FeS}$ ) [24].

In the processing of  $\text{PbS}$  ores by flotation, the  $\text{PbS}$  surface undergoes oxidation and carbonation by dissolved oxygen and carbon dioxide. Various oxides have been reported to form on the surface namely  $\text{PbSO}_4$ ,  $\text{PbCO}_3$  and  $\text{PbS}_2\text{O}_3$  [6–8]. To float the  $\text{PbS}$ , xanthates with 2–5 carbon atoms in the alkyl chain are commonly used. The adsorption of xanthates on  $\text{PbS}$  has been extensively studied, and two adsorption mechanisms have been postulated: (1) chemisorption of xanthate ions on surface  $\text{Pb}$ -sites and (2) ionic exchange between xanthate ions and carbonate, sulfate or thiosulfate species [8, 9]. Very little is known about the thermochemistry of the adsorption mechanisms,

✉ A. López-Valdivieso  
alopez@uaslp.mx

<sup>1</sup> Instituto de Metalurgia, Universidad Autónoma de San Luis Potosí, Av. Sierra Leona 550, 78210 San Luis Potosí, Mexico

<sup>2</sup> Instituto de Física, Universidad Autónoma de San Luis Potosí, Av. Manuel Nava 6, 78290 San Luis Potosí, Mexico

# Synthesis, characterization, and toxicity of hollow gold nanoshells

Sayma Adriana Rodriguez-Montelongo · Jesus Gonzalez-Hernandez · Abel Hurtado Macias · Ana Sonia Silva-Ramirez · Claudia G. Castillo Martin del Campo · Jose Manuel Gutierrez-Hernandez · Facundo Ruiz · Omar Gonzalez-Ortega 

Received: 6 June 2018 / Accepted: 13 November 2018 / Published online: 22 November 2018  
© Springer Nature B.V. 2018

**Abstract** Hollow gold nanoshells (HGN) with a diameter of 50–70 nm and tunable optical properties within the near-infrared region were synthesized from a substitution reaction using a sacrificial template, in which the morphological properties of the HGN were affected by the synthesis conditions. Using EDX line scan, the composition of the structure was determined to verify if the sacrificial template is completely consumed or residues remain after the chemical synthesis, obtaining that the final HGN structure contains about 11% of the

remaining silver that showed no significant effect on the cell viability of a hNS1 cell line, but resulted as toxic on a C6 glioma cell line at high concentrations. The photothermal properties were evaluated using a NIR laser, which despite its low power showed the conversion of light into heat. This study was conducted to evaluate the potential of these nanostructures as therapeutic agents with an emphasis on toxicity.

**Keywords** Photothermal therapy · Hollow gold nanoshells · Surface plasmon resonance · EDX line scan · Toxicity · Silver residues

S. A. Rodriguez-Montelongo · F. Ruiz  
Facultad de Ciencias, Universidad Autonoma de San Luis Potosi,  
Salvador Nava Ave, no number, 78290 San Luis Potosi, Mexico

J. Gonzalez-Hernandez  
Centro de Ingenieria y Desarrollo Industrial, 702 Playa Pie de la  
Cuesta Ave, 76130 Queretaro, Mexico

A. H. Macias  
Centro de Investigacion en Materiales Avanzados, 120 Miguel de  
Cervantes St, 31136 Chihuahua, Mexico

A. S. Silva-Ramirez · O. Gonzalez-Ortega (✉)  
Facultad de Ciencias Quimicas, Universidad Autonoma de San  
Luis Potosi, 6 Manuel Nava Ave, 78210 San Luis Potosi, Mexico  
e-mail: omar.gonzalez@uaslp.mx

C. G. Castillo Martin del Campo  
Facultad de Medicina, Universidad Autonoma de San Luis Potosi,  
2405 Venustiano Carranza Ave, 78210 San Luis Potosi, Mexico

J. M. Gutierrez-Hernandez  
Coordinacion para la Inovacion y la Aplicacion de la Ciencia y la  
Tecnologia, Universidad Autonoma de San Luis Potosi, 550 Sierra  
Leona Ave, 78210 San Luis Potosi, Mexico

## Introduction

Metallic nanoshells are one of the most interesting and potentially useful materials that have been recently developed (Hao et al. 2004). Among these, hollow gold nanoshells (HGN) can be outlined, which are produced from the reaction between  $\text{HAuCl}_4$  and silver nanoparticles (SNP) or cobalt nanoparticles (CNP) in an aqueous environment (Kim et al. 2008). CNP as a sacrificial template have been reported by Schwartzberg et al. and others (Liang et al. 2005; Lindley et al. 2017; Schwartzberg et al. 2006). The synthesis is carried out by reducing  $\text{CoCl}_2$  in the presence of sodium borohydride and sodium citrate as reducing and capping agents, respectively. It is necessary to remove dissolved oxygen from the solution by purging with nitrogen or argon to reduce premature oxidation caused by ambient conditions (Olson et al. 2008; Preciado-Flores et al.



# Detection of hydroquinone by Raman spectroscopy in patients with melasma before and after treatment

R. Cabrera-Alonso<sup>1</sup> | E. Guevara<sup>1,2</sup> | M. G. Ramírez-Elías<sup>3</sup> | B. Moncada<sup>4</sup> | F. J. González<sup>1</sup>

<sup>1</sup>Terahertz Science and Technology Center (C2T2) and Terahertz Science and Technology National Lab (LANCYTT), Universidad Autónoma de San Luis Potosí, San Luis Potosí, México

<sup>2</sup>CONACYT- Universidad Autónoma de San Luis Potosí, San Luis Potosí, México

<sup>3</sup>Facultad de Ciencias, Universidad Autónoma de San Luis Potosí, San Luis Potosí, México

<sup>4</sup>Dermatology Department, Hospital Central 'Dr. Ignacio Morones Prieto', Universidad Autónoma de San Luis Potosí, San Luis Potosí, México

## Correspondence

E. Guevara, CONACYT-Universidad Autónoma de San Luis Potosí, San Luis Potosí, México.  
Email: edgar.guevara@uaslp.mx

## Funding information

Dermatology Department of the Hospital Central 'Dr. Ignacio Morones Prieto'; Consejo Nacional de Ciencia y Tecnología, Grant/Award Number: Doctoral Grant and Project 528 Cátedras; Terahertz Science and Technology National Lab (LANCYTT)

## Abstract

**Background:** Melasma is an acquired, facial hyperpigmentation without a specific origin. It is regularly associated with multiple etiologic factors such as pregnancy, genetic, racial, and from estrogen administration. Among the methods to treat skin hyperpigmentation a series of skin bleaching agents have been used. At present, the most commonly used agent is known as hydroquinone. Nowadays, it is known that hydroquinone can cause cancer in animals with unknown relevance to humans.

**Material and Methods:** In this work, Raman spectroscopy was used to observe the presence of hydroquinone in the skin of 18 patients who have been under treatment for melasma.

**Results:** A significant increase in the Raman signal was observed in the six bands associated with hydroquinone after melasma treatment.

**Conclusion:** The authors believe that monitoring the presence of hydroquinone may be useful for an optimal personalized treatment of melasma and to provide the specialist a support tool to control the administration of this type of bleaching agents.

## KEYWORDS

hydroquinone, melasma, non-invasive diagnostics, Raman spectroscopy

## 1 | INTRODUCTION

Hydroquinone is an aromatic compound in the form of light tan to gray crystals. It is used as a skin bleaching agent, in cosmetics, hair dye, glue, and as medication to treat melasma. Hydroquinone is biodegradable but can be toxic to microorganisms at high concentrations.<sup>1</sup> People using commercial skin lighteners containing hydroquinone developed a blue- or brownish-blue-colored skin. Effects on the kidney, liver, and forestomach, including cancer, were found in laboratory rats fed hydroquinone in the diet or in water.<sup>1</sup> In 1999, the International Agency for Research on Cancer determined that hydroquinone did not possess carcinogenic properties in humans. This decision was based on limited data in animal models and lack of evidence in humans. In 2014, the American Conference

of Governmental Industrial Hygienists decided that hydroquinone is confirmed to cause cancer in animals with unknown relevance to humans, although a 2 mg/m<sup>3</sup> exposure guideline was recommended per workshift<sup>1</sup>. This compound has not endured a full assessment under the US EPA's IRIS (Integrated Risk Information System, prepared and maintained by the Environmental Protection Agency of the United States of America) program for evidence of cancer risk to humans.<sup>1</sup>

Nevertheless, monitoring the presence of this substance at high concentrations in the skin of patients who have been under clinical lightening treatments for melasma could be useful for future carcinogenesis studies. These days, critical innovative advances have been accomplished at the intersection of scientific and technological fields, such as optics, materials science, medicine and electronics.



**Recibido:** 13 de julio del 2017  
**Aceptado:** 7 de mayo del 2018  
**Publicado:** 6 de noviembre del 2018

### Cómo citar:

Hernández Arteaga, L. O., Loreda Tovias, M., Araujo Martínez, R., Compeán Jasso, M. E., de Alba Montero, I. & Ruiz, F. (2018). Determination of silver concentration in tomato seeds (*Solanum Lycopersicum* L.) exposed to silver nanoparticles using AAS-F and a validated method. *Acta Universitaria*, 28(5), 58-65. doi: 10.15174/au.2018.2024

## Determination of silver concentration in tomato seeds (*Solanum Lycopersicum* L.) exposed to silver nanoparticles using AAS-F and a validated method

### Determinación de la concentración de plata en semillas de tomate (*Solanum Lycopersicum* L.) expuestas a nanopartículas de plata utilizando AAS-F y un método validado

Luis Octavio Hernández Arteaga\*\*, Marcos Loreda Tovias\*\*, René Araujo Martínez\*\*, Martha Eugenia Compeán Jasso\*, Idania de Alba Montero\*\*, Facundo Ruiz\*\*

\* Instituto Potosino de Investigación Científica y Tecnológica, A.C.(IPICYT). Camino a la Presa San José 2055. Col. Lomas 4a. CP. 78216. San Luis Potosí S.L.P. México. Telephone: (444) 8262300, Ext. 2396 o 2924. Email: martha.compean@gmail.com.

\*\* Universidad Autónoma de San Luis Potosí.

° Corresponding author.

### Keywords:

Tomato seeds; uptake; silver nanoparticles.

### Palabras Clave:

Semillas de tomate; absorción; nanopartículas de plata.


## ABSTRACT

The interaction of silver nanoparticles with Tomato seeds (*Solanum Lycopersicum* L.) was studied; the amount of silver uptake by tomato seeds was quantified by using flame atomic absorption. The absorption analysis was carried out according to the performance study of the method to estimate the detection and quantification limits as well as the accuracy. The seeds were exposed at different silver concentrations and different times. A simple method has been developed for the determination of silver content in aqueous matrices by acid digestion followed by atomic absorption spectroscopy flame; it was found that the acid digestion is efficient for extraction of the analyte in a single step. The limits of quantification achieved in the analytical method allow the determination of silver on plant tissue, the highest silver uptake in the tomato seeds was obtained with the treatment using the highest silver concentration (10 mM) and longer exposition time (48 h).

## RESUMEN

Se estudió la interacción de nanopartículas de plata con semillas de tomate (*Solanum Lycopersicum* L.); la cantidad de plata absorbida por las semillas se cuantificó usando absorción atómica de flama. Se realizó un estudio de rendimiento del método para determinar los límites de detección y de cuantificación así como la reproducibilidad. Las semillas se expusieron a diferentes concentraciones de plata y diferentes tiempos. Se desarrolló un método simple para la determinación del contenido de plata en matrices acuosas mediante digestión ácida seguida de espectroscopia de absorción atómica de flama; encontrándose que la digestión ácida es eficiente para la extracción del analito. Los límites de cuantificación obtenidos en el método analítico permiten la determinación de la plata en muestras de tejido vegetal, obteniendo la mayor absorción de plata en las semillas de tomate con el tratamiento de mayor concentración (10 mM) y mayor tiempo (48 h).

# SCIENTIFIC REPORTS



OPEN

## Maximally nonlocal Clauser-Horne-Shimony-Holt scenarios

Jesús Urías & José Manuel Méndez Martínez

The key feature in correlations established by multi-party quantum entangled states is nonlocality. A quantity to measure the average nonlocality, distinguishing it from shared randomness and in a direct relation with no-signaling stochastic processes (which provide an operational interpretation of quantum correlations, without involving information transmission between the parties as to sustain causality), is proposed and resolved exhaustively for the quantum correlations established by a Clauser-Horne-Shimony-Holt setup (or CHSH box). The amount of nonlocality that is available in a CHSH box is measured by its proximity to the nearest Popescu-Rohrlich set of causal stochastic processes (aka a PR box) in the no-signaling polytope, related by polyhedral duality to Bell's correlation function. The proposed amount of average nonlocality is an entanglement monotone with a simple relation to concurrence. We provide the optimal setup vectors of a maximally nonlocal CHSH box for any entangled pair. The strongest nonlocality is the fraction  $\frac{\sqrt{2}-1}{2} \approx 0.414$  of a PR box, attained by maximally entangled qubit pairs. The most economical causal stochastic process reproducing any maximally nonlocal CHSH box is developed. Data produced by a computer implementation of the simulator agrees with the quantum mechanical formulas.

The interest in quantum correlations as an information-processing resource<sup>1-3</sup> puts under consideration the problem of finding the experimental setup that maximizes the strength of non-locality that is achievable from a given multi-party quantum state being shared in a Bell scenario. But first, how to size up the strength of the non-locality that might be present in quantum correlations<sup>4</sup>?

In a bipartite (finite ab initio) Bell scenario involving two dichotomic measurements per party (a Clauser-Horne-Shimony-Holt (CHSH) setup<sup>5</sup> for short) quantum correlations may be stronger than just shared classical information, implying that an instant form of causal (non-communicating) nonlocality between the two party locations is involved. Thus, if no communication between the parties is supported, what is the physical resource that is responsible for non-locality in quantum bipartite setups? Entanglement is necessary but it is certainly not enough.

The measure of a physical setup as a resource is determined by the largest operational outcome that, in principle, the physical setup is able to provide. Traditionally, the interest was to distinguish classical from quantum correlations in Bell scenarios and it was then natural to quantify non-locality as the maximum violation of a Bell inequality allowed by a given quantum state. Nowadays, operational interests in quantum information theory might decide about the unit to quantify non-locality resources. The current views on Bell nonlocality are reviewed in<sup>6</sup> and the resource-theory point of view in<sup>4</sup>. Currently, the PR-box is a choice<sup>7</sup> to measure the amount of non-locality that is supplied by bipartite setups sharing qubit pairs.

The PR-box is an elementary (but hypothetical) building block in probability theory that combines causality and nonlocality in one unit. It was first advanced by Popescu and Rohrlich (PR)<sup>8</sup> and then was proved elementary in the no-signaling formalism<sup>6</sup>. The PR box has become a new information-theoretic entity with the clear meaning of a non-reducible (atomic) form of causal (non-communicating) nonlocality. For instance, an unlimited number of PR boxes (together with a fixed amount of classical communication) allows two parties to give a simple solution to any communication complexity problem<sup>9</sup>.

Our theoretical framework for non-locality in quantum correlations in finite setups is the no-signaling formalism. This choice leaves off the discussion any form of noncausal non-locality: classical communication does not have a place in the formalism. Any *finite* causal-correlational setup—as the CHSH setup—is characterized in the no-signaling formalism by a point in the polytope of no-signaling stochastic matrices (or no-signaling boxes). The no-signaling polytope for the CHSH setup is cut by the CHSH inequalities producing the CHSH facets. The vertices the cuts leave outside are the nonlocal PR boxes. The skeleton of the CHSH polytope was computed in<sup>10</sup> and the adjacency of PR boxes in the skeleton is given in Table A2 of the Appendix. Table A2 shows that every PR box is the apex of an 8-simplex with a CHSH facet as its base.

Instituto de Física, UASLP, San Luis Potosí, SLP, Mexico. Correspondence and requests for materials should be addressed to J.U. (email: [jurias@fisica.uaslp.mx](mailto:jurias@fisica.uaslp.mx))

## Research Article

# Cytotoxic and Bactericidal Effect of Silver Nanoparticles Obtained by Green Synthesis Method Using *Annona muricata* Aqueous Extract and Functionalized with 5-Fluorouracil

María del Carmen Sánchez-Navarro,<sup>1</sup> Claudio Adrian Ruiz-Torres <sup>2</sup>,  
Nereyda Niño-Martínez,<sup>2</sup> Roberto Sánchez-Sánchez,<sup>3</sup>  
Gabriel Alejandro Martínez-Castañón <sup>2</sup>, I. DeAlba-Montero,<sup>2</sup> and Facundo Ruiz <sup>2</sup>

<sup>1</sup>Facultad de Estomatología, Universidad Autónoma de San Luis Potosí (UASLP), Avenida Manuel Nava 2, Zona Universitaria, 78290 San Luis Potosí, Mexico

<sup>2</sup>Facultad de Ciencias, Universidad Autónoma de San Luis Potosí (UASLP), Avenida Manuel Nava 6, Zona Universitaria, 78290 San Luis Potosí, Mexico

<sup>3</sup>Instituto Nacional de Rehabilitación LGII, CENIAQ, Calzada México Xochimilco No. 289, Colonia Arenal de Guadalupe, Delegación Tlalpan, 14389 Ciudad de México, Mexico

Correspondence should be addressed to Claudio Adrian Ruiz-Torres; [ruiztorresclaudio@gmail.com](mailto:ruiztorresclaudio@gmail.com) and Facundo Ruiz; [ruizfacundo1@gmail.com](mailto:ruizfacundo1@gmail.com)

Received 30 May 2018; Accepted 6 September 2018; Published 15 October 2018

Guest Editor: Aurel Tabacaru

Copyright © 2018 María del Carmen Sánchez-Navarro et al. This is an open access article distributed under the Creative Commons Attribution License, which permits unrestricted use, distribution, and reproduction in any medium, provided the original work is properly cited.

Nanomaterials obtained by green synthesis technologies have been widely studied in recent years owing to constitute cost-effective and environmental-friendly methods. In addition, there are several works that report the simultaneous performance of the reducer agent as a functionalizing agent, modifying the properties of the nanomaterial. As a simple and economical synthesis methodology, this work presents a method to synthesize silver nanoparticles (AgNPs) using *Annona muricata* aqueous extract and functionalized with 5-fluorouracil (5-FU). The processes of reduction, nucleation, and functionalization of the nanoparticles were analyzed by UV-Vis absorption spectroscopy, and it was found that they are the function of the contact time of the metal ions with the extract. The structural characterization was carried out by transmission electron microscopy (TEM) and X-ray diffraction patterns (XRD). The antibacterial properties of the synthesized nanomaterials were tested using minimum inhibitory concentration (MIC) and minimum bactericidal concentration (MBC) against *Enterococcus faecalis*, *Staphylococcus aureus*, and *Escherichia coli* growth.

## 1. Introduction

The use of nanoparticles as nanodelivery vehicles has received quite great interest in the medical sector in recent years owing to the fact that, by biochemical engineering, it is possible to design multifunctional nanostructured biomaterials to deliver specific drugs to target tumor or cancer cells [1]. The best performance of nanobiomaterials with respect to other types of biomaterials is due to quite high compatibility and adaptability to biological systems, which additionally represents nonviral systems, constituting

promising tools in biomedicine research. A clear example of this fact is silver nanoparticles; due to the application of these types of materials to biological systems, there has been development of numerous nanodelivery vehicles, in view of their intrinsic properties, biocompatibility, and antimicrobial capacity [2]. It is necessary to improve material properties and biocompatibility for a more efficient yield in drug delivery to a specific target, avoiding a wide distribution of the medicine. In light of this, the material functionalization and organometallic science by the development of covalent nets or polymeric functionalization have modified the



## Full Length Article

## A simple method for fabrication of antifuse WORM memories

J.A. Ávila-Niño<sup>a,b,c</sup>, M. Reyes-Reyes<sup>b</sup>, O. Núñez-Olvera<sup>b</sup>, R. López-Sandoval<sup>a,\*</sup><sup>a</sup> Advanced Materials Department, IPICYT, Camino a la Presa San José 2055, Col. Lomas 4a sección, San Luis Potosí 78216, Mexico<sup>b</sup> Instituto de Investigación en Comunicación Óptica, Universidad Autónoma de San Luis Potosí, Álvaro Obregón 64, San Luis Potosí 78000, Mexico<sup>c</sup> CONACYT - Centro de Investigación y Desarrollo en Electroquímica, Parque Tecnológico Querétaro s/n Sanfandila, Pedro Escobedo, Querétaro 76703, Mexico

## ARTICLE INFO

## Keywords:

Aluminium oxide  
UV-ozone treatment  
WORM memories  
polyvinyl alcohol layer

## ABSTRACT

A write-only-read-many (WORM) memory device was obtained by irradiating, with a commercial ultraviolet-ozone (UVO) lamp, the aluminium bottom electrode in an Al/AlO<sub>x</sub>-UVO/Al configuration. The formation of conductive paths due Joule heating is observed when a positive or negative bias voltage is applied to the device, occurring a permanent transition from high (OFF) to low (ON) resistance state. After OFF to ON transitions, physical deformations were observed on the top of the devices, which were analyzed using morphological studies of the top electrode. To eliminate these physical deformations, the UVO treatment on the aluminium bottom electrode was replaced by the deposition of a thin polyvinyl alcohol (PVA) film (10 nm). These Al/AlO<sub>x</sub>-native/PVA/Al WORM memories presented similar I-V behaviours and the same threshold voltages to those Al/AlO<sub>x</sub>-UVO/Al devices, but with higher ON/OFF ratios. Analysis of the I-V curves confirms that the same physical phenomena, such as the formation of filamentary paths, are occurring for both types of devices.

## 1. Introduction

Resistive memory devices consist generally in an active layer embedded between two metallic electrodes, which are able to change between a high resistance state (OFF) and low resistance state (ON). In the case of a permanent change from OFF and ON, these memory devices are named write once read many times (WORM) memories, whereas when these memory devices can change several times between the OFF and ON they named rewritable memories. One of the main advantages of resistive memories, in comparison with the most common memories used in electronic components, is that they are nonvolatile, i.e. these retain information even if the power is turned off [1]. In particular, WORM memories have potential applications in ultra-low cost digital storage [2] and other permanent digital storage applications for video, images, electronic voting and non-editable database [3,4].

Nonvolatile memory behaviour has been observed for different organic and inorganic [5] composites used as active layers. WORM memories have been reported for metal/dielectric polymer/metal devices generally with polymer thickness < 100 nm [6]. It has been considered for several groups that the presence of an oxide film is the responsible for obtaining resistive switching in WORM memories [3,7,8]. Among the inorganic materials showing rewritable or WORM characteristics are several oxide films such as TiO<sub>2</sub> [9] and Al<sub>2</sub>O<sub>3</sub> [10]. These oxides are deposited by different methods that are expensive and,

in some cases, can involve temperature, like sputtering [11] and atomic layer deposition [12]. Sometimes, it is only necessary a thin oxide film, created by an oxidation of the surface of electrodes or at the interface between two thin films, for their applications in devices. For these reasons, several electrode-engineering methods like oxygen plasma exposition [13], ultraviolet-ozone (UVO) lamp [14], natural exposition to the atmosphere [15,16] and ozone irradiation [17] have been used in order to obtain a thin oxide film. Using some of these surface modification techniques allow to compare, for example, the differences in the physicochemical properties due to the oxidation of an aluminium thin film by oxygen and ozone [17,18]; it is found that the film irradiated with O<sub>3</sub> showed an increment of the insulating properties related with the increase of the barrier width [19]. Additionally, it has been reported that the irradiation of aluminium films with an UVO lamp improves their insulating properties and diminishes the leakage current in organic thin film transistors [14]. The improvement of the insulating property by ozone irradiation has been observed using other insulator materials like Ta<sub>2</sub>O<sub>5</sub> [20].

In general, the switching mechanism of rewritable memory devices based on aluminium oxides (AlO<sub>x</sub>) can be explained by the formation and destruction of filaments in the aluminium oxide film [4,21]. In the case of WORM memories, the conductive filaments in the oxide film can only be created and not destroyed [3,8,22,23]. Recently, it has been reported Al/Al-rich AlO<sub>x</sub>N<sub>y</sub>/Si WORM memory in devices [8] and, for these devices, it has been argued that oxygen vacancies could generate

\* Corresponding author.

E-mail address: [sandov@ipicyt.edu.mx](mailto:sandov@ipicyt.edu.mx) (R. López-Sandoval).

# Mind-to-mind heteroclinic coordination: Model of sequential episodic memory initiation

V. S. Afraimovich,<sup>1,a)</sup> M. A. Zaks,<sup>2,3</sup> and M. I. Rabinovich<sup>4</sup>

<sup>1</sup>*Instituto de Investigación en Comunicación Óptica, Universidad Autónoma de San Luis Potosí, 78220 San Luis Potosí, Mexico*

<sup>2</sup>*Institute of Physics, Humboldt University of Berlin, 12489 Berlin, Germany*

<sup>3</sup>*Research Institute for Supercomputing, Nizhny Novgorod State University, Nizhny Novgorod, Russia*

<sup>4</sup>*BioCircuits Institute, University of California, San Diego, La Jolla, California 92093-0328, USA*

(Received 26 January 2018; accepted 25 April 2018; published online 10 May 2018)

Retrieval of episodic memory is a dynamical process in the large scale brain networks. In social groups, the neural patterns, associated with specific events directly experienced by single members, are encoded, recalled, and shared by all participants. Here, we construct and study the dynamical model for the formation and maintaining of episodic memory in small ensembles of interacting minds. We prove that the unconventional dynamical attractor of this process—the nonsmooth heteroclinic torus—is structurally stable within the Lotka-Volterra-like sets of equations. Dynamics on this torus combines the absence of chaos with asymptotic instability of every separate trajectory; its adequate quantitative characteristics are length-related Lyapunov exponents. Variation of the coupling strength between the participants results in different types of sequential switching between metastable states; we interpret them as stages in formation and modification of the episodic memory. *Published by AIP Publishing.* <https://doi.org/10.1063/1.5023692>

**Our ability to graft images and ideas into the minds of other humans is crucial for the existence of science, technology, and literature. Participation of a community member in an event or group of events (episode) suffices to implant the memory of that episode into the minds of the whole community. In our daily life, we take this ability for granted, but only the recent advances of measurement technique have disclosed how, e.g., a movie spectator encodes and transfers *a posteriori* to listeners the neural patterns associated with viewing specific episodes and how these event-specific patterns are shared among the brains. In the large-scale networks of the individual brain, a retrieval of episodic memory occurs in a way of sequential switching between the events, the perpetual “winnerless competition.” We propose and investigate the mathematical model for the formation and maintaining of common memory in interacting minds. By combining rigorous proofs with numerical studies, we show that weak coupling between the participant’s minds ensures the existence of the so-called “attracting heteroclinic torus” in the phase space of the model. Changing the coupling strength, we observe different types of dynamics that correspond to various forms of episodic memory.**

Development of technology and science, as well as the sheer existence of oral and written literature owes much to the fact that personal participation in an event is not a necessary precondition of keeping that event in one’s memory: humans are able to mentally construct episodes when reading or listening to recollections of other humans. A recent study, based on analysis of magnetic resonance brain imaging during the performance of verbal communication tasks, traced how neural patterns associated with viewing specific scenes in a movie were encoded, recalled, and then transferred to a group of listeners who had not seen the movie.<sup>1</sup> It disclosed that event-specific patterns, observed in the brain default mode network, were shared across the processes of encoding, recalling, and constructing the same episodes. Such studies uncover intimate correspondences between episodic memory encoding and construction and underscore the role of the common language in the transmission of memory to other brains.

Communication in persistent social groups (families, friends, colleagues, etc.) is facilitated by common episodic memories: interpersonal knowledge of past, shared by the group members.<sup>2</sup> Distributed within the group, such memories serve as a stem around which new layers of shareable information are accumulated. Notably, episodic memories are not exact replicas of the lives: rather, they are organized summaries of experience, encoded in the form of sequential groups of events.<sup>3</sup> According to the recent imaging data, the brain areas responsible for storage and retrieval of episodic memories include hippocampus, striatum, and the prefrontal cortex.<sup>4,5</sup>

## I. INTRODUCTION

*Even across different languages, our brains show similar activity, or become “aligned” when we hear the same idea or story. This amazing neural mechanism allows us to transmit brain patterns, sharing memories and knowledge.*

*Uri Hasson (2016).*

## II. LOW-DIMENSIONAL MIND DYNAMICS

Below, we present and study a low-dimensional model of mind-to-mind episodic memory interaction. We

<sup>a)</sup>Deceased

# Relationship between the passivation of TiO<sub>2</sub> particles and LLDPE photodegradation: a comparison between bulk and surface impacts

Blanca E. Castillo-Reyes <sup>1</sup>, Zoe V. Quiñones-Jurado,<sup>1</sup> R. Catarino-Centeno,<sup>2,3</sup>  
J. Roberto López-Jiménez,<sup>4</sup> Elías Pérez<sup>5</sup>

<sup>1</sup>Innovación y Desarrollo en Materiales Avanzados, A.C., Grupo Polynnova, Carretera San Luis Potosí - Guadalajara 1510, Fraccionamiento Lomas del Tecnológico, 78211, San Luis Potosí, SLP, Mexico

<sup>2</sup>Posgrado en Ciencias Aplicadas, Facultad de Ciencias, Universidad Autónoma de San Luis Potosí, Álvaro Obregón 64, 78000, San Luis Potosí, SLP, Mexico

<sup>3</sup>División de Ingeniería Mecatrónica, Instituto Tecnológico Superior de Zacapoaxtla, Tecnológico Nacional de México, Carretera Acuaco-Zacapoaxtla, km 8, Col. Toltepec, 73680, Zacapoaxtla, Puebla, Mexico

<sup>4</sup>A Schulman de México S.A. de C.V., Av. Comisión Federal de Electricidad 730, Industrial San Luis, 78395, San Luis Potosí, SLP, Mexico

<sup>5</sup>Instituto de Física, Universidad Autónoma de San Luis Potosí, Álvaro Obregón 64, 78000, San Luis Potosí, SLP, Mexico  
Correspondence to: Tel.: +52 4448262362, Ext.134. E. Pérez (E-mail: elias@ifisica.uaslp.mx) and B.E. Castillo-Reyes (E-mail: becr\_jq@yahoo.com.mx)

**ABSTRACT:** The effect of the concentration of alumina (Al<sub>2</sub>O<sub>3</sub>) and silica (SiO<sub>2</sub>) used to passivate titanium dioxide (TiO<sub>2</sub>) particles on the photodegradation of plastic films containing these particles was investigated. The films were made of linear low-density polyethylene (LLDPE) containing four different types of passivated TiO<sub>2</sub> particles. The UV degradation of the films was evaluated for the surface and the bulk by measuring the physical and chemical changes as a function of time. The surface chemical and physical degradation effects were measured by ATR-FTIR and AFM, respectively. A statistical Gaussian adjustment was proposed to correlate the AFM depth profiles of the eroded surfaces of the films after the photodegradation process. The bulk physical effect was evidenced by the loss of mechanical properties in the films. The results showed that the higher the concentrations of Al<sub>2</sub>O<sub>3</sub> are, the better the inhibition of the photodegradation of the LLDPE films. In this study, it was confirmed that the observed UV degradation effect correlated at both the surface and bulk levels. The results showed not only the reduction of the photodegradative effect as the passivation of the TiO<sub>2</sub> particles increased but also the possibility of using these particles as UV stabilizers of LLDPE films. © 2018 Wiley Periodicals, Inc. *J. Appl. Polym. Sci.* 2019, 136, 47026.

Received 29 December 2017; accepted 13 July 2018

DOI: 10.1002/app.47026

## INTRODUCTION

Titanium dioxide (TiO<sub>2</sub>) is mostly used as a white pigment in the production of white plastics due to its high refractive index. When the TiO<sub>2</sub> particles are added to a polymer, a higher light scattering is produced.<sup>1</sup> In this context, TiO<sub>2</sub> has been used in a wide variety of industrial applications, including packaging materials, protective filters, membranes, agricultural equipment, and automotive and building parts.<sup>2–4</sup> However, the application of TiO<sub>2</sub> is limited to outdoor environments, especially over long time periods, since TiO<sub>2</sub> can degrade the polymer by photodegradation.<sup>5–8</sup> In plastics, this unfavorable degradation is observed through the loss of mechanical and optical properties.

It is known that TiO<sub>2</sub> generates free holes and electrons upon exposure to ultraviolet (UV) light, which lead to the creation of

reactive species that rapidly destroy organic materials. In polymers, rutile TiO<sub>2</sub> is preferred over anatase because the latter accelerates the photooxidative degradation of the polymer due to its high oxidation potential.<sup>9,10</sup> However, even rutile TiO<sub>2</sub> particles need to be passivated to diminish their photocatalytic properties.

To reduce rutile reactivity, TiO<sub>2</sub> particles are typically passivated by metallic oxides,<sup>11,12</sup> and the passivated effect can be improved by using amine hindered light stabilizers (HALS).<sup>13–15</sup> TiO<sub>2</sub> particles are commonly coated with individual or mixtures of metallic oxides, such as alumina (Al<sub>2</sub>O<sub>3</sub>), silica (SiO<sub>2</sub>), and zirconia (ZrO<sub>2</sub>).<sup>11,16</sup> Passivation is evidently dependent on factors such as particle geometry, crystal type, particle size distribution and effective surface area.<sup>9–11,17–23</sup> Until now, there has been a lack of



## Full Length Article

# On the origin of reflectance-anisotropy oscillations during GaAs (001) homoepitaxy

J. Ortega-Gallegos<sup>a,\*</sup>, L.E. Guevara-Macías<sup>a</sup>, A.D. Ariza-Flores<sup>a,b</sup>, R. Castro-García<sup>a,b</sup>, L.F. Lastras-Martínez<sup>a</sup>, R.E. Balderas-Navarro<sup>a</sup>, R.E. López-Estopier<sup>a,b</sup>, A. Lastras-Martínez<sup>a</sup>

<sup>a</sup> Instituto de Investigación en Comunicación Óptica, Universidad Autónoma de San Luis Potosí, Alvaro Obregón 64, San Luis Potosí, SLP 78000, Mexico

<sup>b</sup> CONACyT - Instituto de Investigación en Comunicación Óptica, Universidad Autónoma de San Luis Potosí, Alvaro Obregón 64, San Luis Potosí, SLP 78000, Mexico

## ARTICLE INFO

## Article history:

Received 25 October 2017

Revised 22 December 2017

Accepted 28 December 2017

Available online 6 January 2018

## Keywords:

Reflectance anisotropy oscillations

Real-time measurements

GaAs homoepitaxy

## ABSTRACT

We report on the first spectroscopic study of reflectance-anisotropy (RA) oscillations during molecular beam epitaxy (MBE) GaAs homoepitaxy. Real-time RA spectra measured during epitaxial growth were carried out with a recently developed rapid RA multichannel spectrometer with 100 ms per spectrum acquisition time. An analysis of the time-resolved RA spectra shows that RA oscillations are mostly due to the periodic modulation of the surface orthorhombic strain associated to surface reconstruction. Results reported here demonstrate the power of real-time RA spectroscopy as a probe for the study of epitaxial growth processes. In particular, given its sub monolayer surface-strain sensitivity, RA spectroscopy results a very convenient tool to study epitaxial growth mechanisms in real-time with sub monolayer resolution. This capability allows for real-time RA spectroscopy to be used as a probe for the *in situ*, real-time control of epitaxial growth, with the additional advantage of operating in higher pressure systems such as CVD, where RHEED monitoring cannot be implemented.

© 2018 Elsevier B.V. All rights reserved.

## 1. Introduction

The fabrication of advanced optoelectronic devices based on zincblende semiconductors demands for probes with both real-time monitoring and feedback control capabilities for the epitaxial growth process with at least monolayer (ML) resolution. Optical probes would be advantageous for this application given their instrumental simplicity and provided we overcome their intrinsic low surface specificity. Reflectance anisotropy (RA) is an optical polarization contrast technique which enhances the surface-related response by taking advantage of the reduced symmetry of the surface or near surface region of the crystal. RA measures the difference in the optical reflectivity between two principal axis of the crystal, thus suppressing the polarization-independent bulk signal and enhancing the surface response [1].

RA has been applied to study the kinetics of the epitaxial growth of various zincblende semiconductors, demonstrating high sensitivity to the different stages of the growth process [2,3]. In particular, it is known that the intensity of the RA signal oscillates during growth with the same oscillation period as that of specular

RHEED oscillations [4], which is known to correspond to the time necessary to grow one monolayer. RHEED oscillations are widely accepted to be associated to periodic changes in surface micro roughness that take place during layer-by-layer growth [5]. Phenomena leading to RA oscillations, in contrast, are not fully understood. In this regards, on the basis of an effective medium model, Aspnes argues that optical anisotropies associated to surface roughness are too small to explain experimental results and concludes that they have a surface chemistry origin [6]. RA oscillations have also been explained on the basis of a modulation of As dimer coverage during growth as dimers are preferentially broken at island edges [7].

Previous determinations of RA oscillations have been carried out at a single-wavelength or at most a few wavelengths [3,4,7]. However, as it has been shown elsewhere, RA signals may comprise more than one independent component [8,9], hence hampering the physical interpretation of RA oscillations on the basis of single-wavelength data. A deeper understanding of RA oscillations thus demands time-resolved spectroscopic measurements. Carrying out such measurements, nevertheless, demand a rapid RA spectrometer, fast enough to follow in real-time the kinetics of epitaxial growth of III-V compounds (spectrum acquisition times of the order of 0.1 s and  $\Delta R/R$  amplitude in the range  $10^{-3}$ ). Harrison et al., developed a 16 channel rapid RA spectrometer to study the

\* Corresponding author.

E-mail addresses: [jortega@cactus.iico.uaslp.mx](mailto:jortega@cactus.iico.uaslp.mx) (J. Ortega-Gallegos), [alastras@gmail.com](mailto:alastras@gmail.com) (A. Lastras-Martínez).

# Orthorhombic Distortion in Au Single-Crystal Nanoparticles Subjected to High Pressure

Rubén Mendoza-Cruz<sup>1\*</sup>; Prakash Parajuli<sup>1</sup>; H. Joazet Ojeda-Galván<sup>2</sup>, Lourdes Bazán-Díaz<sup>1</sup>; J. Jesús Velázquez-Salazar<sup>1</sup>; and Miguel José-Yacamán<sup>1\*</sup>.

<sup>1</sup> Department of Physics & Astronomy, University of Texas at San Antonio, One UTSA Circle, San Antonio, TX 78249, United States of America.

<sup>2</sup> Coordinación para la Innovación y la Aplicación de la Ciencia y la Tecnología (CIACYT), Universidad Autónoma de San Luis Potosí (UASLP), Álvaro Obregón 64, 78000 San Luis Potosí, México.

\*Corresponding Authors





# Use of Raman spectroscopy to screen diabetes mellitus with machine learning tools

EDGAR GUEVARA,<sup>1,2,\*</sup> JUAN CARLOS TORRES-GALVÁN,<sup>2</sup> MIGUEL G. RAMÍREZ-ELÍAS,<sup>3</sup> CLAUDIA LUEVANO-CONTRERAS,<sup>4</sup> AND FRANCISCO JAVIER GONZÁLEZ<sup>2</sup>

<sup>1</sup>CONACYT-Universidad Autónoma de San Luis Potosí, Mexico

<sup>2</sup>Terahertz Science and Technology Center (C2T2) and Science and Technology National Lab (LANCyTT), Universidad Autónoma de San Luis Potosí, Mexico

<sup>3</sup>Facultad de Ciencias, Universidad Autónoma de San Luis Potosí, Mexico

<sup>4</sup>Department of Medical Sciences, University of Guanajuato, Leon, Mexico

\*[eguevara@conacyt.mx](mailto:eguevara@conacyt.mx)

**Abstract:** Type 2 diabetes mellitus (DM2) is one of the most widely prevalent diseases worldwide and is currently screened by invasive techniques based on enzymatic assays that measure plasma glucose concentration in a laboratory setting. A promising plan of action for screening DM2 is to identify molecular signatures in a non-invasive fashion. This work describes the application of portable Raman spectroscopy coupled with several supervised machine-learning techniques, to discern between diabetic patients and healthy controls (Ctrl), with a high degree of accuracy. Using artificial neural networks (ANN), we accurately discriminated between DM2 and Ctrl groups with 88.9–90.9% accuracy, depending on the sampling site. In order to compare the ANN performance to more traditional methods used in spectroscopy, principal component analysis (PCA) was carried out. A subset of features from PCA was used to generate a support vector machine (SVM) model, albeit with decreased accuracy (76.0–82.5%). The 10-fold cross-validation model was performed to validate both classifiers. This technique is relatively low-cost, harmless, simple and comfortable for the patient, yielding rapid diagnosis. Furthermore, the performance of the ANN-based method was better than the typical performance of the invasive measurement of capillary blood glucose. These characteristics make our method a promising screening tool for identifying DM2 in a non-invasive and automated fashion.

© 2018 Optical Society of America under the terms of the [OSA Open Access Publishing Agreement](#)

**OCIS codes:** (170.5660) Raman spectroscopy; (170.4580) Optical diagnostics for medicine; (070.5010) Pattern recognition

## References and links

1. World Health Organization, “Global Report on Diabetes,” [www.who.int/diabetes/global-report](http://www.who.int/diabetes/global-report).
2. IQWiG (Institute for Quality and Efficiency in Health Care), “Defunciones por diabetes mellitus por entidad federativa y grupo quinquenal de edad según sexo, 2010 a 2015,” [http://www.beta.inegi.org.mx/app/tabulados/pxweb/inicio.html?rxid=75ada3fe-1e52-41b3-bf27-4cda26e957a7&db=Mortalidad&px=Mortalidad\\_4](http://www.beta.inegi.org.mx/app/tabulados/pxweb/inicio.html?rxid=75ada3fe-1e52-41b3-bf27-4cda26e957a7&db=Mortalidad&px=Mortalidad_4).
3. IQWiG (Institute for Quality and Efficiency in Health Care), “Type 2 diabetes: Overview” (PubMed Health, 2014).
4. R. T. Demmer, A. M. Zuk, M. Rosenbaum, and M. Desvarieux, “Prevalence of diagnosed and undiagnosed type 2 diabetes mellitus among US adolescents: results from the continuous NHANES, 1999-2010,” *Am. J. Epidemiol.* **178**(7), 1106–1113 (2013).
5. J. Beagley, L. Guariguata, C. Weil, and A. A. Motala, “Global estimates of undiagnosed diabetes in adults,” *Diabetes Res. Clin. Pract.* **103**(2), 150–160 (2014).
6. M. I. Harris and R. C. Eastman, “Early detection of undiagnosed diabetes mellitus: a US perspective,” *Diabetes Metab. Res. Rev.* **16**(4), 230–236 (2000).
7. J. F. Villa-Manríquez, J. Castro-Ramos, F. Gutiérrez-Delgado, M. A. López-Pacheco, and A. E. Villanueva-Luna, “Raman spectroscopy and PCA-SVM as a non-invasive diagnostic tool to identify and classify qualitatively glycosylated hemoglobin levels in vivo,” *J. Biophotonics* **10**(8), 1074–1079 (2016).

# Antimycotic Activity Potentiation of *Allium sativum* Extract and Silver Nanoparticles against *Trichophyton rubrum*

Marissa Robles-Martínez,<sup>a</sup> Juan Fernando Cárdenas González,<sup>b</sup> Francisco Javier Pérez-Vázquez,<sup>c</sup> Juan Martín Montejano-Carrizales,<sup>d</sup> Elías Pérez,<sup>\*d</sup> and Rosalba Patiño-Herrera<sup>\*e</sup>

<sup>a</sup> Doctorado en Ingeniería y Ciencia de Materiales de la UASLP, Sierra Leona 530, San Luis Potosí, San Luis Potosí 78210, México

<sup>b</sup> Unidad Académica Multidisciplinaria Zona Media, UASLP, Rioverde, San Luis Potosí 79617, México

<sup>c</sup> Coordinación para la Innovación y Aplicación de la Ciencia y la Tecnología (CIACYT), UASLP, San Luis Potosí, San Luis Potosí 78210, México

<sup>d</sup> Instituto de Física, UASLP, Álvaro Obregón 64, San Luis Potosí 78000, México, e-mail: elias@ifiscia.uaslp.mx

<sup>e</sup> Departamento de Ingeniería Química, Tecnológico Nacional de México/Instituto Tecnológico de Celaya, Antonio García Cubas Pte #600 esq. Av. Tecnológico. Celaya, Guanajuato 38010, México, e-mail: roos\_ph@iqcelaya.itc.mx

A natural and biocompatible extract of garlic as a support, decorated with silver nanoparticles, is a proposal to generate an effective antifungal agent against dermatophytes at low concentrations. Silver nanoparticles (AgNPs) with a diameter of  $26 \pm 7$  nm were synthesized and their antimycotic activity was examined against *Trichophyton rubrum* (*T. rubrum*), inhibiting 94% of growth at a concentration of  $0.08 \text{ mg ml}^{-1}$ . *Allium sativum* (garlic) extract was also obtained (AsExt), and its MIC was  $0.04 \text{ mg ml}^{-1}$ . To increase the antifungal capacity of those systems, AsExt was decorated with AgNPs, obtaining AsExt-AgNPs. Using an AsExt concentration of  $0.04 \text{ mg ml}^{-1}$  in independent experiments with concentrations from 0.01 to  $0.08 \text{ mg ml}^{-1}$  of AgNPs, it was possible to inhibit *T. rubrum* at all AgNPs concentrations; it proves a synergistic effect between AgNPs and AsExt. Even if 1% of the minimum inhibitory concentration of AsExt ( $0.0004 \text{ mg ml}^{-1}$ ) is used, it was possible to inhibit *T. rubrum* at all concentrations of AgNPs, demonstrating the successful antimycotic activity potentiation when combining AsExt and AgNPs.

**Keywords:** antimycotic activity, potentiation, *Allium sativum* (garlic), silver nanoparticles, *Trichophyton rubrum*, biological activity.

## Introduction

Dermatophytes are common on tropical regions due to high humidity levels. During 2008, the rate of this fungal infection worldwide prevalence was of 20 to 25%,<sup>[1]</sup> hair keratin, skin and nails are its food source. The ability of dermatophytes to infect a host depends on several factors such as skin moisture, a slightly acidic pH, continuous skin regeneration, fatty acid conditions, keratinized state layer and the normal skin microbiota competition.<sup>[2]</sup> Infection begins with inoculation of spores deposited on a skin lesion or abrasion and its enzymatic ability to degrade keratin.<sup>[3]</sup> The

main dermatophytes that affect humans are *Epidermophyton*, *Microsporum* and *Trichophyton*.<sup>[4]</sup> Onychomycosis, also called tinea unguium or dermatophytic onychomycosis, is a fungal infection that damages the nail and skin nail union, and it affects about 10% of the adult population. This infection is caused mainly by *Trichophyton rubrum*, *Trichophyton mentagrophytes*, *T. interdigitale*, *Epidermophyton floccosum*, *T. violaceum*, *Microsporum gypseum*, *T. tonsurans* and *T. soudanense*.<sup>[5]</sup> Orally ingested medication that usually prescribed are griseofulvin, azole group different drugs (itraconazole, fluconazole, albaconazole, posaconazole, ravuconazole) and terbinafine. Nevertheless, there are



## Pushing HSI to the Limit for the Quantification of Peanut Traces in Bulk Powder Foods

Pilar Barreiro<sup>1\*</sup>, Belén Diezma<sup>1</sup>, Teresa R. Cuadrado Dominguez<sup>1</sup>, Inés María López-Calleja<sup>2</sup>, Lourdes Lleó<sup>1</sup>, Ana Herrero-Langreo<sup>3</sup>, Puneet Mishra<sup>1</sup>, Satyabrata Ghosh<sup>1</sup>, Eva Cristina Correa<sup>1</sup>, Teresa García<sup>2</sup>, Nathalie Gorretta<sup>3</sup>, SitiNurHidayah Mohamad<sup>1</sup>, Pablo Delgado Sánchez<sup>5</sup>, Facundo Ruiz<sup>6</sup>, Christophe B.Y. Cordell<sup>6</sup>, Douglas N. Rutled<sup>6</sup>, Jean Michel Roger<sup>3</sup>, Rosario Martínde Santos<sup>2</sup> and Margarita Ruiz-Altisent<sup>1</sup>

<sup>1</sup>LPF\_TAGRALIA Departamento de Ingeniería Agroforestal, UPM CEI Moncloa, Madrid, España

<sup>2</sup>Departamento de Nutrición, Bromatología y Tecnología de los Alimentos, Facultad de Veterinaria, Universidad Complutense de Madrid, 28040 Madrid, Spain

<sup>3</sup>Irstea, UMR ITAP, 361 Rue J. F. Breton, 34196 Montpellier Cedex 5, France

<sup>4</sup>AgroParisTech UMR1145 Genial, Analytical Chemistry Laboratory, 16 rue Claude Bernard, F-75005 Paris, France <sup>5</sup>Facultad de Agronomía y Veterinaria, UASLP, San Luis Potosí, México

<sup>5</sup>Facultad de Agronomía y Veterinaria, UASLP, San Luis Potosí, México

<sup>6</sup>Facultad de Ciencias, UASLP, San Luis Potosí, México

Received March 1, 2018; Accepted March 26, 2018; Published June 26, 2018

### REVIEW

#### CEI Moncloa as the Origin of this Interdisciplinary Research

The CEI\_Moncloa was a proposal coordinated by the Complutense University of Madrid (UCM) and the Technical University of Madrid (UPM), approved in 2011, in which 13 institutions have been integrated. It houses around 10,000 researchers, 10% of the national scientific production and approximately 80,000 students (75% of the

UCM and 25% of the UPM), including the Agri-Food and Health Cluster. It is situated in the so-called Agroalimentary Corridor, which groups together the activities that all these groups carry out in the production of agricultural and livestock products, and their subsequent processing for the creation of safe, healthy and nutritious food and feed. In this context we have been committed to finding synergistic and stable relations among research groups and as a consequence of a think tank set up to do this, there has been a steady scientific production since the first published works in 2014 (**Figure 1**).

**Corresponding Author:** Pilar Barreiro, LPF\_TAGRALIA Departamento de Ingeniería Agroforestal, UPM CEI Moncloa, Madrid, España, Email: pilar.barreiro@upm.es

**Citation:** Barreiro P, Diezma B, Dominguez TRC, Calleja IML, Lleó L, et al., (2018) Pushing HSI to the Limit for the Quantification of Peanut Traces in Bulk Powder Foods. Food Nutr Current Res, 1(2): 56-60.

**Copyright:** ©2018 Barreiro P, Diezma B, Dominguez TRC, Calleja IML, Lleó L, et al. This is an open-access article distributed under the terms of the Creative Commons Attribution License, which permits unrestricted use, distribution, and reproduction in any medium, provided the original author and source are credited.

## Economía, geometría y dinámica

Elvio Accinelli\*

(Recibido: septiembre 2017/Aceptado: febrero 2018)

### Resumen

El presente trabajo pretende mostrar cómo la geometría diferencial y los sistemas dinámicos permiten entender, explicar y avanzar en el estudio de problemas económicos relevantes. Pretendemos convencer al lector de que una teoría formalmente desarrollada puede no estar muy lejos de la práctica más inmediata y que, por otra parte, los problemas que la realidad cotidiana nos plantea pueden ser un excelente pretexto para dedicarnos a la más abstracta teoría.

El artículo está destinado a un amplio público, en particular a las personas interesadas en la Teoría Económica y particularmente en la Economía Matemática. No obstante, aspiramos a que, matemáticos y economistas provenientes de áreas diferentes, encuentren en él, un incentivo para futuros estudios en la temática. Esperamos que el objetivo declarado no esté muy lejos de los resultados alcanzados.

*Palabras claves:* equilibrio walarasiano, dinámica del subastador, variedad de equilibrios.

*Clasificación JEL:* D5; C61; C62.

---

\* El autor desea agradecer al M. en C. Ricardo Hernández Medina por su apoyo para la edición del presente documento y a la Maestra Mara del Huerto Bettini por la corrección de la redacción. Facultad de Economía, UASLP México. Correo electrónico: elvio.accinell@eco.uaslp.mx

# Almost congruence extension property for subgroups of free groups

Lev Glebsky and Nevarez Nieto Saul

Communicated by Alexander Olshanskii

**Abstract.** Let  $H$  be a subgroup of  $F$  and  $\langle\langle H \rangle\rangle_F$  the normal closure of  $H$  in  $F$ . We say that  $H$  has the Almost Congruence Extension Property (ACEP) in  $F$  if there is a finite set of nontrivial elements  $F \subset H$  such that for any normal subgroup  $N$  of  $H$  one has  $H \cap \langle\langle N \rangle\rangle_F = N$  whenever  $N \cap F = \emptyset$ . In this paper, we provide a sufficient condition for a subgroup of a free group to not possess ACEP. It also shows that any finitely generated subgroup of a free group satisfies some generalization of ACEP.

## 1 Introduction

Let  $X$  be a group. We use the following standard notations:  $Y < X$  for “ $Y$  is a subgroup of  $X$ ”,  $Y \triangleleft X$  for “ $Y$  is a normal subgroup of  $X$ ”,  $\langle Y \rangle$  for “the subgroup generated by  $Y$ ”,  $\langle\langle Y \rangle\rangle_X$  for “the normal closure of  $Y$  in  $X$ ”. (In the last two cases, one has  $Y \subseteq X$ .)

**Definition 1.** Let  $F$  be a group. A subgroup  $H$  of  $F$  has the Congruence Extension Property (CEP) if for any normal subgroup  $N$  of  $H$  one has  $H \cap \langle\langle N \rangle\rangle_F = N$ .

The CEP is known by different names. Ol’shanskii [10] calls it property  $F(n)$ , B. H. Neumann [8] names subgroups with the CEP as E-subgroups, Stallings [13] calls them normal convex subgroups and, finally, Osin [11] introduces the self-explaining name CEP. It is worth mentioning that the term CEP was used before for subalgebras and subsemigroups. A natural question is: when does a subgroup  $H$  of a group  $F$  possess CEP? The question seems difficult, even when  $H$  is a finitely generated subgroup of a free group  $F$ . Particularly, its algorithmic decidability is, as far as we know, an open question. An obvious example of a subgroup with

---

Part of this work was done at the Erwin Schrödinger Institute in Vienna, January-March 2016, during the Measured Group Theory program and was partially supported by the European Research Council (ERC) grant no. 259527 of G. Arzhantseva. Part of this work was done at the Nizhny Nivgorod University and supported by the RSF (Russia) grant 14-41-00044.



# Synthesis of bactericidal polymer coatings by sequential plasma-induced polymerization of 4-vinyl pyridine and gas-phase quaternization of poly-4-vinyl pyridine

Martha Hernández-Orta<sup>1</sup> , Elías Pérez<sup>2</sup> , Luis Emilio Cruz-Barba<sup>3</sup> , and Marco A. Sánchez-Castillo<sup>1,4,\*</sup> 

<sup>1</sup> Facultad de Ciencias Químicas, Universidad Autónoma de San Luis Potosí, Manuel Nava 6, 78210 San Luis Potosí, S.L.P., Mexico

<sup>2</sup> Instituto de Física, Universidad Autónoma de San Luis Potosí, Manuel Nava 6, 78210 San Luis Potosí, S.L.P., Mexico

<sup>3</sup> Departamento de Ingeniería Química-CUCEI, Universidad de Guadalajara, Marcelino García Barragán 1421, 44430 Guadalajara, Jal, Mexico

<sup>4</sup> Coordinación para la Innovación y la Aplicación de la Ciencia y la Tecnología, Universidad Autónoma de San Luis Potosí, Sierra Leona 550, 78210 San Luis Potosí, S.L.P., Mexico

Received: 24 October 2017

Accepted: 27 February 2018

Published online:

12 March 2018

© Springer Science+Business Media, LLC, part of Springer Nature 2018

## ABSTRACT

Plasma-based technology is an alternative to produce universal polymer coatings with the appropriate requirements of robustness and stability for antibacterial applications. Here, we proposed a sequential two-step alternative to synthesize antibacterial polymer coatings. A non-isothermal plasma reactor, operated at atmospheric pressure ( $P_{\text{atm}}$ ) and room temperature ( $T_{\text{room}}$ ), was used to induce free radical polymerization of 4-vinyl pyridine (4VP) on high-density polyethylene (PE). In a subsequent step, the poly-4VP (P4VP) films were treated with a bromoethane/He gas stream to produce quaternized P4VP (P4VPQ) films. Chemical structure of polymer films was validated by infrared and UV–visible spectroscopy, and morphology was evaluated by optical and atomic force microscopy; scanning electron microscopy was used to determine films thickness, which was then used to estimate the surface charge density. The bactericidal capacity was determined with a standard test by using *Escherichia coli*. Both types of films had an estimated charge density in the order of  $10^{16}$  positive charges per  $\text{cm}^2$ ; P4VP films removed about 95–99% of bacteria, whereas P4VPQ films eliminated 100%. The methodology proposed for the synthesis of antibacterial polymer coatings is simpler, faster, and more environmentally friendly than other plasma-based methods; operation at  $T_{\text{room}}$  and  $P_{\text{atm}}$  may also have a significant effect on the economics and the ease of implementation of the process at commercial scale. The suggested approach may facilitate the development of new universal coatings, and operating plasma conditions could be extrapolated for engineering antibacterial coatings in industrial areas where bacterial attachment is of concern.

Address correspondence to E-mail: masanchez@uaslp.mx



# Gold Nanoparticle: Enhanced CO Oxidation at Low Temperatures by Using Fe-Doped TiO<sub>2</sub> as Support

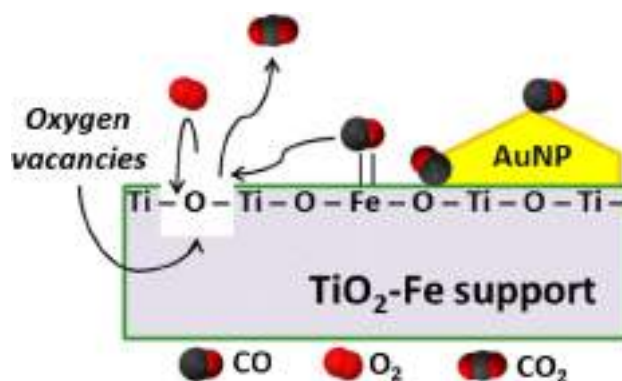
Mariana Hinojosa-Reyes<sup>1</sup> · Roberto Camposeco-Solis<sup>2</sup> · Rodolfo Zanella<sup>3</sup> · Vicente Rodríguez-González<sup>2</sup> · Facundo Ruiz<sup>1</sup>

Received: 3 October 2017 / Accepted: 19 November 2017 / Published online: 29 November 2017  
© Springer Science+Business Media, LLC, part of Springer Nature 2017

## Abstract

Iron doped TiO<sub>2</sub> materials were prepared by the sol–gel method and used as supports of gold nanoparticles synthesized by the deposition–precipitation technique. The gold–iron–titania catalysts were characterized by X-ray diffraction, Raman spectroscopy, N<sub>2</sub> physisorption, UV–Vis spectroscopy as a function of temperature, H<sub>2</sub>-temperature programmed reduction, transmission electronic microscopy and X-ray photoelectron spectroscopy. The gold–iron catalysts were catalytically active during the CO oxidation reaction at low temperatures, reaching CO conversion percentages of almost 80% at room temperature. The Au/TiO<sub>2</sub>–Fe catalyst surface was characterized through infrared spectroscopy (DRIFTS) during the CO oxidation reaction to elucidate the active sites and the real carbon monoxide interaction during the reaction. A 24-h deactivation test corroborated a final deactivation of the catalysts of only 25% for both Au/TiO<sub>2</sub>–Fe 1 and the bare Au/TiO<sub>2</sub>. The results here obtained corroborate that the activity of the iron-doped TiO<sub>2</sub> catalyst was higher than that of the bare TiO<sub>2</sub> due to the iron incorporation into the TiO<sub>2</sub> lattice, which allows the formation of surface oxygen vacancies and new adsorption sites which favor the CO adsorption and its oxidation to CO<sub>2</sub>.

## Graphical Abstract



**Keywords** Heterogeneous catalysis · DRIFTS · XPS · Deposition–precipitation · Sol–gel · CO oxidation

## 1 Introduction

The properties of nanometric gold supported on different metallic oxides and its good performance in the CO oxidation reaction were discovered by Haruta et al. [1]. Since this discovery, gold nanoparticles (AuNPs) have been deposited on different metallic oxides with different redox properties to

✉ Mariana Hinojosa-Reyes  
kittyhinojosa@hotmail.com

Extended author information available on the last page of the article



## Synthesis and Characterization of Hydrogels with Ag Nanoparticles

K. G. H Martínez-Reyna; M. G. García-Valdivieso; H. R. Navarro-Contreras

Laboratorio Nacional CIACYT-Universidad Autónoma de San Luis Potosí, Av. Sierra Leona 550, Col. Lomas 2a. Sección, C.P 78210, San Luis Potosí, S.L.P., MÉXICO.

### ABSTRACT

*Hydrogels made of sodium 2-acrylamide-2-methylpropanesulfonate were synthesized with the goal of creating a polymer for tissue engineering applications. The hydrogels were doped with silver nanoparticles to create hydrogel/Ag with possible antibacterial properties. We varied the weight/volume percentage of Laponite from 3 to 10 w/v% to alter the rheological properties of the hydrogels. Raman spectroscopy was used to study the progress of the chemical reaction at different polymerization times under ultraviolet radiation. By comparing the changes in the intensities of the Raman bands corresponding to C=C and C–C bonds with reaction time, we found that the optimal polymerization time to obtain chains of poly(2-acrylamide-2-methylpropanesulfonate) was 3 to 4 h. Characterization of the hydrogels with scanning electron microscopy indicated pore sizes of 1 to 6  $\mu\text{m}$ .*

### INTRODUCTION

Hydrogels are of great interest because of their unique properties, including ability to absorb large volumes of water, softness, flexibility and biocompatibility [1]. Hydrogels are three-dimensional, hydrophilic, polymeric networks capable of absorbing large amounts of water or biological fluids. Based on these properties, hydrogels have numerous applications in drug delivery, pesticides and tissue engineering. Tissue engineering is a method used to regenerate damaged tissue or replace organs in the body [2]. For example, injuries to menisci are the second most common knee injury, with an incidence of 61 cases per 100,000 persons [3]. This injury is common in young people (under 40 years) and especially athletes, along with patients over 65 years of age [4]. Currently, meniscus injuries are treated using transplants. While Verdonk et al. reported that 75%–90% of patients experienced fair to excellent functional results after meniscal



Karina Cruz-Rodríguez<sup>a</sup>, Ricardo García-Alamilla<sup>a</sup>, Francisco Paraguay-Delgado<sup>b</sup>,  
María-Guadalupe Cárdenas-Galindo<sup>c</sup>, Brent E. Handy<sup>c</sup>, Juan Reyes-Gómez<sup>d</sup>

<sup>a</sup>Centro de Investigación en Petroquímica, Instituto Tecnológico de Ciudad Madero, Altamira, Tamps, México.

<sup>b</sup>Centro de Investigación en Materiales Avanzados, Chihuahua, Chih., México.

<sup>c</sup>Universidad Autónoma de San Luis Potosí, San Luis Potosí, Slp., México.

<sup>d</sup>Universidad de Colima, Facultad de Ciencias, Colima, Col., México.

# Lewis–Brønsted induction acidity in SBA-15 modified with Zr and P

In this work, we present the synthesis of SBA-15 materials modified with 6 and 9 mol.% of Zr and P, respectively. Silanol SBA-15 groups were detected by Fourier transform infrared spectroscopy. X-ray diffractograms revealed that the typical hexagonal arrangement of SBA-15 was preserved after Zr and P introduction, and the structure was confirmed by transmission electron microscopy. After the Zr introduction, the morphology of SBA-15 changed from fibrous particles to a semi-spherical shape according to scanning electron microscopy, while nitrogen physisorption revealed the stability of the textural materials after the P introduction. The infrared spectra of pyridine adsorption indicated that the Zr and P incorporation into SBA-15 generated adequate Lewis and Brønsted acidities to carry out methanol dehydration and direct the selectivity towards dimethyl ether, with medium-strong acid sites being responsible for obtaining up to 99% selectivity towards dimethyl ether.

**Keywords:** SBA-15; ZrO<sub>2</sub>; PO<sub>4</sub><sup>3-</sup>; Methanol; Dimethyl ether

## 1. Introduction

Several mesoporous materials, such as Santa Barbara amorphous No. 15 (SBA-15) and mobil composition of matter No. 41 (MCM-41), have received an abundance of attention for catalytic applications because of their textural properties, such as well-defined pore size and shape, large pore volume (0.5–2.5 cm<sup>3</sup> g<sup>-1</sup>) and pore size (4.6–30 nm), and high surface area (500–1500 m<sup>2</sup> g<sup>-1</sup>) [1]. SBA-15 possesses the advantage of being more stable thermally and hydrothermally than MCM-41 [2, 3]. Unfortunately, its lack of acidity is a disadvantage when it is considered for applications such as alcohol dehydration, dehydrogenation, cumene cracking, and n-paraffin isomerization [4–6]. Several studies have described that acid sites are generated in SBA-15 by the replacement of silicon atoms with metal ions, such as zirconium and aluminum, as well as sulfate [7, 8]. However, in most cases, the introduction of these agents affects the textural properties of the mesoporous material, reducing its surface area by up to 68% [9, 10] or collapsing its hexagonal structure [11].

Phosphate species have also been used to generate acid sites, although their role either as a stabilizer or as a promoter is not yet well understood [12]. However, it is known that they have a better thermal stability than do sulfate species. These acid sites are lost at operating conditions near 873 K [13, 14], whereas the phosphate species remain above this temperature [15]. Thermal stability is thus an advantage that phosphates have over sulfates, mainly in their ability to tolerate the regeneration processes required to reactivate carbon-poisoned catalysts [16] in dehydration reactions or in the isomerization of n-paraffins.

Some research groups have demonstrated that the incorporation of phosphate in ZrO<sub>2</sub> improves its textural properties and surface acidity [17, 18]. Parida and Pattnayak [19] reported that the textural and acidic properties of PO<sub>4</sub><sup>3-</sup>/ZrO<sub>2</sub> at concentrations of 1–4 wt.% PO<sub>4</sub><sup>3-</sup> are greater than the area and acidity of pure ZrO<sub>2</sub>, a result of the phosphate incorporation. However, at concentrations higher than 4 wt.% PO<sub>4</sub><sup>3-</sup>, both the area and acidity of the materials decrease due to the formation of polyphosphates, which reduce the number of Brønsted acid sites and consequently the total acid sites.

It has been reported in several studies that solid catalysts with acidic characteristics are required in the methanol dehydration to dimethyl ether (DME). This compound is an attractive alternative fuel because its combustion is clean, and it can be produced from various sources, including natural gas and even biomass [20, 21]. In particular, Dong et al. [9] reported that the introduction of zirconium to SBA-15 generates Brønsted and Lewis acid sites, which catalyze methanol dehydration at approximately 623 K, obtaining up to 90% selectivity towards DME. However, they reported that the specific area of SBA-15 is reduced upon zirconium addition by more than 60% because of the formation of ZrO<sub>2</sub> nanoparticles within the pores of the SBA-15 structure. A similar effect was reported for the addition of aluminum to SBA-15 [10].

However, although most of the catalysts employed in methanol dehydration are highly active, they have the disadvantage of promoting the formation of light olefins, which tend to polymerize by forming and depositing carbonaceous residues on the catalyst surface [22, 23]. For instance, Fu et al. [24] reported that catalysts constituted of SiO<sub>2</sub>/Al<sub>2</sub>O<sub>3</sub> are highly active in methanol decomposition but generate a large diversity of carbon precursor by-products that deactivate the catalysts in a very short time.

## Comparative Study of CdS and CdS/ZnS Thin Films Deposited by CBD as a Buffer Layer Solar Cell

A. García-Barrientos<sup>1</sup>, H. Gomez-Pozos<sup>2</sup>, E. Villicaña-Ortiz<sup>3</sup> and L. Cruz-Netro<sup>4</sup>

<sup>1</sup>. Faculty of Science, Universidad Autónoma de San Luis Potosí, SLP, México.

<sup>2</sup>. Electronics Department, Universidad Autónoma del Estado de Hidalgo, Hidalgo, México.

<sup>3</sup>. Departamento de Ingeniería de la Energía, Universidad de Ingeniería y Tecnología, Lima, Peru

<sup>4</sup>. Ingeniería Industrial, Universidad Politécnica de Altamira, México

Cadmium sulphide (CdS) and Cadmium sulphide/Zinc sulfide (CdS/ZnS) thin films have been extensively investigated as an *n*-type buffer layer to form thin film heterojunction solar cells with *p*-CdTe absorber layers. The buffer layer affects the electrical properties of the junction and protects it from chemical reactions. From the electronic point of view, the CdS and CdS/ZnS layers can optimize the band alignment of the device [1 and 2]. Also, these can build a sufficiently wide depletion width that minimizes tunneling and establishes a higher contact potential that allows higher open circuit voltage [2]. Recently, a particular attention of the researches has been focused on the heterostructures involving CdS and CdS/ZnS multilayers [3]. Because of its band gap, it could be an excellent window layer in CdTe thin film solar cells. Since Chemical Bath Deposition (CBD) is known to produce solar cells over a large area at a low cost and low temperature. The effect of deposition parameters of CdS and CdS/ZnS thin films developed by CBD technique were investigated in [4 and 5], principally, the influence of pH control of the reaction solution on the structural and optical properties of chemically deposited CdS and CdS/ZnS thin films. Different films thicknesses of CdS and CdS/ZnS thin films were deposited onto a glass substrate. The structural surface morphology of as-deposited CdS and CdS/ZnS thin films was characterized by SEM. The physical conditions were kept identical while growing of the samples. The investigation of the effect of the synthesis method on the change the ammonium hydroxide by buffer pH (from 10.1 - 13) contributed in increases the growth kinetics, resulting in thicker films.

In this paper, a comparative study of CdS and CdS/ZnS thin films deposited by CBD as a buffer layer solar cell was carried out. The CdS and CdS/ZnS thin films were fabricated by CBD technique on a glass substrate for a deposition time of 60 minutes at a bath temperature of 90 °C. These thin films were synthesized by chemical bath deposition using acid as a complexing agent with pH values between 10.1 to 11.3 for the CdS thin films and for the CdS/ZnS thin films with pH values between 11.4 to 13, these can be seen in the Figures 1a and 1b, respectively. The SEM photos (see figure 1a) show the surfaces of CdS films grown at 60 minutes deposition time and to different solution pH values. Based on the optical transmission measurements, the square of absorption coefficient ( $\alpha^2$ ) is plotted as a function of photon energy ( $h\nu$ ) in figure 1c, one can see the energy band gap,  $E_g$ , values 2.38, 2.58 and 2.44 eV for pH values, 10.1, 10.6 and 11.3, respectively. In the other case, for the CdS/ZnS thin films grown at 60 minutes time deposition, one can see the SEM photos of the samples surfaces in the figure 1c. Also, we found different energy band gaps for different pH values; for pH=11.4,  $E_g$  equals 2.74 eV and at pH=11.8,  $E_g$  equals 2.7 eV, these values are pretty similar of the literature [6]. Finally, these studies show that the pH contributes noticeably to the growth and to the structure of deposited CdS and CdS/ZnS multilayer films. This may be interpreted by the decrease of the film thickness. From these studies, we are able to optimize the process in order to produce the layer suitable for optical window in solar cells. For the case of CdS thin films, it is better to use acid as a complexing agent with pH value equal to 10.6 and for the case of CdS/ZnS thin films, it is better use with pH value equal to 11.4. This approach could be used in improving the spectral response of CdTe-based solar cells. A higher band gap was observed for CdS/ZnS, it indicates that there is clear short-wavelength advantages in current

## Numerical Analysis Receiving/Transmitting Mechanisms of ZnO/Ag Nanoantennas

A. García-Barrientos<sup>1</sup>, F. R. Castillo-Soria<sup>1</sup>, M. A. Cardenas-Juarez<sup>1</sup>, V. I. Rodríguez-Abdala<sup>2</sup>, F. J. Gonzalez<sup>3</sup> and J. E. Sánchez<sup>3</sup>

<sup>1</sup> Faculty of Science, Universidad Autónoma de San Luis Potosí, SLP, Mexico.

<sup>2</sup> Department of Electronics and Communications, Universidad Autónoma de Zacatecas, Mexico

<sup>3</sup> LANCYTT, Universidad Autónoma de San Luis Potosí, SLP, Mexico

The fabrication, characterization and numerical analysis receiving/transmitting mechanisms of ZnO/Ag nanoantennas are very important nowadays, because it is in the group II–VI metal oxide semiconductor with a wide direct band gap [1]. Semiconductor nanostructures are desirable for the modern electronics, nanophotonics, quantum circuitry, plasmonics and energy conversion applications as well as for fundamental science. Specially, in nanophotonics and plasmonics, optical nanoantennas can reduce the breach between photons and semiconductor emitters or detectors in nanoscale. Electrical and optical characteristics of ZnO films are pretty similar like GaN, ZnS, and compound semiconductors, and also because this material has different applications such as solid-state light sources and detectors in the blue and UV spectral range [2-3]. For applications in electronics and optics field, ZnO has interesting properties such as magnetic, piezoelectric, and semiconductor. It has a high electrical conductivity and a high optical gain at ambient temperature. In consequence by these properties, thin films ZnO has found numerous potential applications in fields such as, light emitting diodes, most gas sensors, and solar cells. For example, in the ref. [4] was reported the crystalline orientation analysis at the ZnO/Ag interface, where ZnO rods grown on lateral faces of the pentagonal cross sectional area of silver nanowires were assembled in a hierarchical nanoantenna. This kind of nanoantenna is a promising alternative of plasmonic rf-nanoantennas for engineering light emission because of their low-loss nature in the spectrum [5-7].

In this paper, the numerical analysis receiving/transmitting mechanisms of ZnO/Ag nanoantennas was carried out. In this case, a Yagi-Uda, with 11 elements, type nanoantenna was used to simulate the radiation patterns from 1-5 GHz. In the figure 1, we can see the SEM images of the ZnO thin films (a) and ZnO/Ag hierarchical nanoantennas (b), reported in the ref. [4], where the pentagon geometry can be seen. In the figure 2, we can see the optimized antenna pattern at the design frequency at 5 GHz (a), and to obtain a better insight into the behavior in the two orthogonal planes, we also plotted the normalized magnitude of the electric field in the E and H-planes, i.e. azimuth = 0 (b) and 90 (c) deg, respectively. The results show that the nanoantennas might be capable of transmitting and/or receiving electromagnetic waves when stimulated with a modulated RF signal, especially at high frequency signals.

[1] Jongmin Kim, et al., *Appl. Phys. Lett.*, vol. 102, no. 18, 183901, 2013.

[2] M.A. Contreras, *Thin Solid Films*, vol. 204, 403-404 pp., 2002.

[3] T. Ben Nasr, et al., *Thin Solid Films*, vol. 500, 4-8 pp., 2006.

[4] J. E. Sanchez, et al., *Journal of Applied Physic*, vol. 117, 034306, 2015

[5] Sorias O, et al., *Nano Lett.*, vol. 17(10):6011-6017, 2017

[6] Peter M, et al., *Nano Lett.*, vol. 17(7):4178-4183, 2017



[7] Feng T., et al., *J Phys Condens Matter.*, 2018

The authors acknowledge funding from the CONACYT-Mexico, research projects grant numbers 169062 and 204419. F. J. González would like to acknowledge support from Project 32 of “Centro

# Raman effect in multiferroic $\text{Bi}_5\text{Fe}_{1+x}\text{Ti}_{3-x}\text{O}_{15}$ solid solutions: A temperature study

Cite as: J. Appl. Phys. **123**, 084101 (2018); <https://doi.org/10.1063/1.5019291>

Submitted: 12 December 2017 . Accepted: 05 February 2018 . Published Online: 22 February 2018

Ma. Del Carmen Rodríguez Aranda, Ángel G. Rodríguez-Vázquez , Ulises Salazar-Kuri, María Eugenia Mendoza, and Hugo R. Navarro-Contreras 



View Online



Export Online



CrossMark

## ARTICLES YOU MAY BE INTERESTED IN

[Pressure-induced transformations of multiferroic relaxor  \$\text{PbFe}\_{0.5}\text{Nb}\_{0.5}\text{O}\_3\$](#)

Journal of Applied Physics **123**, 084102 (2018); <https://doi.org/10.1063/1.5019485>

[Thermal annealing and single-domain preparation in tetragonal  \$\text{Pb}\(\text{In}\_{1/2}\text{Nb}\_{1/2}\)\text{O}\_3\$ - \$\text{Pb}\(\text{Mg}\_{1/3}\text{Nb}\_{2/3}\)\text{O}\_3\$ - \$\text{PbTiO}\_3\$  crystal for electro-optic and non-linear optical applications](#)

Journal of Applied Physics **123**, 084104 (2018); <https://doi.org/10.1063/1.5011404>

[The enhanced piezoelectricity in compositionally graded ferroelectric thin films under electric field: A role of flexoelectric effect](#)

Journal of Applied Physics **123**, 084103 (2018); <https://doi.org/10.1063/1.5019446>

Applied Physics Reviews  
Now accepting original research

2017 Journal  
Impact Factor:  
**12.894**



## Detection of *Clavibacter michiganensis* subsp. *michiganensis* Assisted by Micro-Raman Spectroscopy under Laboratory Conditions

Moisés Roberto Vallejo Pérez<sup>1\*</sup>, Hugo Ricardo Navarro Contreras<sup>2</sup>, Jesús A. Sosa Herrera<sup>3</sup>, José Pablo Lara Ávila<sup>4</sup>, Hugo Magdaleno Ramírez Tobías<sup>4</sup>, Fernando Díaz-Barriga Martínez<sup>2</sup>, Rogelio Flores Ramírez<sup>1</sup>, and Ángel Gabriel Rodríguez Vázquez<sup>2</sup>

<sup>1</sup>CONACyT- Universidad Autónoma de San Luis Potosí. Álvaro Obregón #64, Col. Centro, C.P. 78000, San Luis Potosí, S.L.P. México

<sup>2</sup>Universidad Autónoma de San Luis Potosí. Coordinación para la Innovación y la Aplicación de la Ciencia y la Tecnología (CIACyT). Av. Sierra Leona #550, Col. Lomas 2a. Sección, C.P. 78210, S.L.P., México

<sup>3</sup>CONACyT- Centro de Investigación en Ciencias de Información Geoespacial A.C. Circuito Tecnopolo Norte 117, Col. Fraccionamiento Tecnopolo Pocitos, CP. 20313, Aguascalientes, Ags. México

<sup>4</sup>Universidad Autónoma de San Luis Potosí. Facultad de Agronomía y Veterinaria. Km. 14.5 Carretera San Luis Potosí, Matehuala, Ejido Palma de la Cruz, Soledad de Graciano Sánchez, C.P. 78321. S.L.P. México

(Received on February 7, 2018; Revised on May 10, 2018; Accepted on May 31, 2018)

*Clavibacter michiganensis* subsp. *michiganensis* (*Cmm*) is a quarantine-worthy pest in México. The implementation and validation of new technologies is necessary to reduce the time for bacterial detection in laboratory conditions and Raman spectroscopy is an ambitious technology that has all of the features needed to characterize and identify bacteria. Under controlled conditions a contagion process was induced with *Cmm*, the disease epidemiology was monitored. Micro-Raman spectroscopy (532 nm  $\lambda$  laser) technique was evaluated its performance at assisting on *Cmm* detection through its characteristic Raman spectrum fingerprint. Our experiment was conducted with tomato plants in a completely randomized block experimental design (13 plants  $\times$  4 rows). The *Cmm* infection was confirmed by 16S rDNA and plants showed symptoms from 48 to 72 h after inoculation, the evolution of the incidence and severity on plant population varied over time and it kept an aggregated spatial pattern. The contagion pro-

cess reached 79% just 24 days after the epidemic was induced. Micro-Raman spectroscopy proved its speed, efficiency and usefulness as a non-destructive method for the preliminary detection of *Cmm*. Carotenoid specific bands with wavelengths at 1146 and 1510  $\text{cm}^{-1}$  were the distinguishable markers. Chemometric analyses showed the best performance by the implementation of PCA-LDA supervised classification algorithms applied over Raman spectrum data with 100% of performance in metrics of classifiers (sensitivity, specificity, accuracy, negative and positive predictive value) that allowed us to differentiate *Cmm* from other endophytic bacteria (*Bacillus* and *Pantoea*). The unsupervised KMeans algorithm showed good performance (100, 96, 98, 91 y 100%, respectively).

**Keywords** : chemometrics, epidemiology, KMeans, LDA, PCA

**Handling Associate Editor** : Oh, Chang-Sik

\*Corresponding author.

Phone) +52 (444) 826 2300, FAX) +52 (444) 826 8410

E-mail) vallejo.pmr@gmail.com

© This is an Open Access article distributed under the terms of the Creative Commons Attribution Non-Commercial License (<http://creativecommons.org/licenses/by-nc/4.0>) which permits unrestricted noncommercial use, distribution, and reproduction in any medium, provided the original work is properly cited.

Articles can be freely viewed online at [www.ppjonline.org](http://www.ppjonline.org).

The tomato crop (*Solanum lycopersicum* L.) is a domesticated species belonging to the *Solanaceae* family. Taxonomically, it is located in the *Lycopersicon* section alongside 13 related wild species, which can be found on the western coast of South America (Ecuador, Peru, and Chile), this region is considered to be their center of origin; nevertheless, domestication of cultivated tomato occurred

# Real-time Optical Monitoring of Semiconductor Epitaxial Growth

A. Lastras-Martínez<sup>1,a)</sup>, J. Ortega-Gallegos<sup>1</sup>, L.E. Guevara-Macías<sup>1</sup>, D. Ariza-Flores<sup>2</sup>, O. Núñez-Olvera<sup>1</sup>, R.E. López-Estopier<sup>2</sup>, R.E. Balderas-Navarro<sup>1</sup> and L.F. Lastras-Martínez<sup>1</sup>

<sup>1</sup> *Instituto de Investigación en Comunicación Óptica, Universidad Autónoma de San Luis Potosí, San Luis Potosí, México.*

<sup>2</sup> *Cátedras Conacyt, Av. Insurgentes 1582, Crédito Constructor, Delegación Benito Juárez, CDMX 03940, México.*

<sup>a)</sup>Corresponding author: [alastras@gmail.com](mailto:alastras@gmail.com)

**Abstract.** We report on time-resolved Reflectance Anisotropy Spectroscopy (RAS) measurements carried out during the molecular beam epitaxial growth of GaAs (001). Growth started on a c(4x4) reconstructed surface which changed to (2x4) and then to (4x) as growth progressed. We found that reflectance anisotropy spectra comprise three components, each one with a specific physical origin and determine their time evolution as a function of epitaxil film thickness. We conclude that RAS is a powerful probe for the monitoring and potentially for the control of epitaxial growth.


## INTRODUCTION

Light probes, being non-invasive, result very attractive tools for the real-time monitoring of the epitaxial growth of semiconductors. Depending on photon energy, however, light impinging on the substrate penetrates to a depth of 50-500 monolayer, thus limiting surface sensitivity. More than two decades ago, D.E. Aspnes introduced Reflectance-anisotropy spectroscopy (RAS) (also known as Reflectance-difference spectroscopy) which overcomes this limitation by measuring the difference in reflectivity for two mutually orthogonal polarizations [1]. In the past, however, despite the demonstrated RAS surface sensitivity, its use for epitaxial growth monitoring has been hindered by 1) the lack of reflectance anisotropy (RA) spectrometers fast enough to follow atomic processes during growth and 2) the limited understanding of the physics underlining the optical anisotropy of semiconductor surfaces. Here we address these two points and report on time-resolved RAS measurements carried out during the MBE homoepitaxial growth of GaAs (001) that show RAS to be a powerful probe for the monitoring and control of epitaxial growth.

## EXPERIMENTAL

Epitaxial growth was carried out on GaAs (001) substrates in a solid source molecular beam epitaxy chamber (Riber 32P). Growth temperature and As<sub>4</sub> overpressure were set to 520 °C and 2x10<sup>-6</sup> Torr, respectively. With these conditions, during the first growth stage the GaAs film growth rate was 0.19 ML/s, decreasing to 0.13 ML/s as growth stabilized. Prior to RA measurements a 0.2 μm thick undoped GaAs buffer layer was grown on the GaAs substrate. The sample surface is kept under As<sub>4</sub> flux along the whole experiment. Growth is started upon opening the Ga shutter on a c(4x4) reconstructed surface which first changes to (2x4) and then to a Ga-rich reconstruction. As discussed below, the RA spectrum line shape changes substantially along growth.

# Zinc oxide decorated multi-walled carbon nanotubes: their bolometric properties

Guadalupe García-Valdivieso<sup>1,4</sup> , J Jesús Velázquez-Salazar<sup>2</sup>, José Enrique Samaniego-Benítez<sup>3</sup>, Hiram Joazet Ojeda-Galván<sup>1</sup>, M Josefina Arellano-Jiménez<sup>2</sup>, Karí G H Martínez-Reyna<sup>1</sup>, Miguel José-Yacamán<sup>2</sup> and Hugo R Navarro-Contreras<sup>1,4</sup>

<sup>1</sup> Coordinación para la Innovación y la Aplicación de la Ciencia y la Tecnología, Universidad Autónoma de San Luis Potosí, Av. Sierra Leona #550, Col. Lomas 2a. Sección, CP 78210, San Luis Potosí, SLP, México

<sup>2</sup> Department of Physics and Astronomy, University of Texas at San Antonio, San Antonio, TX 78249, United States of America

<sup>3</sup> CINVESTAV-Querétaro, Libramiento Norponiente #2000, Fracc. Real de Juriquilla. C.P. 76230, Querétaro, México

E-mail: [hnavarro@uaslp.mx](mailto:hnavarro@uaslp.mx) and [guadalupe.valdivieso@uaslp.mx](mailto:guadalupe.valdivieso@uaslp.mx)

Received 13 December 2017

Accepted for publication 23 January 2018

Published 12 February 2018



CrossMark

## Abstract

We report the synthesis of MWNT/ZnO hybrid nanostructures. A simple, affordable, chemical procedure to functionalize MWNTs with ZnO nanoparticles was performed. A significant portion of the surface of MWNTs was covered with ZnO nanoparticles; these particles formed highly porous spherical nodules of 50–150 nm in diameter, sizes that are an order of magnitude larger than similar ZnO nanonodules reported in the literature. Hence, the self-assembled nanocomposite the ZnO exhibited a large surface-to-volume ratio, which is a very advantageous property for potential catalytic applications. The resultant MWNT/ZnO nanocomposites were characterized by x-ray diffraction, scanning and high-resolution transmission electron microscopy, and UV–vis and Raman spectroscopy. The temperature coefficient of resistance (TCR) of the nanocomposites was measured and reported. The average TCR value goes from  $-5.6\%/K$  up to  $-18\%/K$ , over temperature change intervals from 10 K to 1 K. Based on these TCR results, the nanocomposite MWNT/ZnO prepared in this work is a promising material, with potential application as a bolometric sensor.

Keywords: multiwalled carbon nanotubes, zinc oxide, nanocomposite, bolometers

(Some figures may appear in colour only in the online journal)

## Introduction

The combination of various materials to form multifunctional hybrid structures has attracted scientific attention due to the unique properties that they present. There is great interest in the development of electronic and sensor devices with new technological applications. One of the properties that hybrid materials possess is that of self-assembly, whereby they adopt new textures and forms. Also, the combination of these materials, presents new possibilities to enhance the response

of conventional bulk materials, in some cases resulting in novel properties [1], thus providing the backbone of future technological advances—which are successful if they surpass the performance of the technology they replace.

Among the available materials, zinc oxide (ZnO) is an excellent candidate for the creation of hybrid materials, since it is a semiconductor with a wide bandgap (3.37 eV at room temperature [2]) and a large excitation binding energy (60 meV [2, 3]), which allow it to have several outstanding physical properties such as high thermal conductivity [2], electrical and chemical stability, and non-toxicity, as well as ferroelectric, pyroelectric and piezoelectric properties [2, 4].

<sup>4</sup> Authors to whom any correspondence should be addressed.

# Rapid Reflectance-Anisotropy Spectroscopy as an Optical Probe for Real-Time Monitoring of Thin Film Deposition

J. Ortega-Gallegos<sup>1,a)</sup>, L. E. Guevara-Macías<sup>1</sup>, A. Lastras-Martínez<sup>1</sup>, D. Ariza-Flores<sup>2</sup>, R.E. Balderas-Navarro<sup>1</sup> and L.F. Lastras-Martínez<sup>1</sup>

<sup>1</sup>*Instituto de Investigación en Comunicación Óptica, Universidad Autónoma de San Luis Potosí, Alvaro Obregón 64, San Luis Potosí, SLP 78000, México Phone: 52 (444) 825 0183, Fax: 52 (444) 825 0198.*

<sup>2</sup>*Cátedras Conacyt, Av. Insurgentes 1582, Crédito Constructor, Delegación Benito Juárez, CDMX 03940, México.*

<sup>a)</sup>Corresponding author: jortega@cactus.iico.uaslp.mx

**Abstract.** We report on real-time spectroscopic reflectance anisotropy measurements carried out during the epitaxial growth of GaAs/GaAs (001). Our work is aimed to the study of fundamental processes occurring during the epitaxial growth of III-V semiconductors. We show that during growth there is an oscillation in the surface strain associated to surface reconstruction, suggesting the existence of a mechanism of periodic build up-relaxation of the surface strain, indicating that the technique employed in this work may potentially distinguish between two reconstruction phases.

## INTRODUCTION

The growth of well controlled surface templates with III-V epitaxy remains a challenge and is a very interesting topic due to their potential applications for nanoscale devices based on GaAs [1, 2]. For this purpose, non-invasive diagnostic probes such as Reflectance-Anisotropy Spectroscopy (RAS) would be of great value. The use of this probe in a feedback control loop would allow for the precise control of surface reconstruction during the for molecular beam epitaxy (MBE) growth. In this regards, it is known that there is close relationship between RAS line shape and surface reconstruction. In the case of the GaAs(001) surface, RAS has proved to be highly sensitive to surface reconstruction, giving information on three types of As-stabilized reconstructions, namely  $\alpha(2 \times 4)$ ,  $\beta(2 \times 4)$  and  $\gamma(2 \times 4)$  [3], and  $\alpha c(4 \times 4)$  and  $\beta c(4 \times 4)$  [4]. It has been reported that RA spectra around  $E_1$  and  $E_1 + \Delta_1$  transitions comprise several components. Among them, we include components induced by surface roughness [5] and surface anisotropic strain fields for both  $c(4 \times 4)$  [6] and  $(2 \times 4)$  surface reconstructions [7]. Such strains are related to a surface stress arising from charge redistribution in the surface bonds due to the absence of atoms above the surface [8]. Reconstruction-induced strain has an orthorhombic symmetry and may penetrates into a region 20 nm thick [6].

Recently, we have shown that it is possible to use real-time RA spectroscopy for monitoring processes taking place during the homoepitaxial growth of GaAs/GaAs (001) [9]. In this paper we report on a real-time RAS investigation of the dynamics of homoepitaxial MBE growth of GaAs (001) at a temperature of 520 °C. Particularly, we focus on the study of RA amplitude oscillations that are linked to the layer by layer growth model. We note that the growth temperature employed in this work is one of the standards in the manufacture of thin films for optoelectronic device applications.

## EXPERIMENTAL DETAILS

Undoped GaAs films were grown on GaAs (001) substrates in a solid source molecular beam epitaxy system (Riber 32P). A home made rapid RA spectrometer attached to the growth chamber enables the acquisition of RA spectra at a rate of 10 spectra/s [10]. The setup allows for the simultaneous measurement of RA spectra and Reflection High Energy Electron Diffraction (RHEED) oscillations during growth. To remove the surface native oxide the GaAs substrate was heated to at a temperature 600 °C until a  $(2 \times 4)$  RHEED pattern was observed. An undoped 0.3  $\mu\text{m}$  thick buffer



# Constant-Length Random Substitutions and Gibbs Measures

C. Maldonado<sup>2</sup>  · L. Trejo-Valencia<sup>1</sup> · E. Ugalde<sup>1</sup> 

Received: 2 December 2017 / Accepted: 6 March 2018  
© Springer Science+Business Media, LLC, part of Springer Nature 2018

**Abstract** This work is devoted to the study of processes generated by random substitutions over a finite alphabet. We prove, under mild conditions on the substitution's rule, the existence of a unique process which remains invariant under the substitution, and which exhibits a polynomial decay of correlations. For constant-length substitutions, we go further by proving that the invariant state is precisely a Gibbs measure which can be obtained as the projective limit of its natural Markovian approximations. We end up the paper by studying a class of substitutions whose invariant state is the unique Gibbs measure for a hierarchical two-body interaction.

**Keywords** Gibbs measures · Random substitutions · Projective convergence

## 1 Introduction

**1.1** The systems we will consider in this work, were introduced to describe the evolution of genome sequences, and in general, are aimed at explaining the pattern correlation that can be observed in real genome sequences. One of the first examples of this kind of systems was proposed by Li [10] as a simple model exhibiting some spatial scaling properties. It was subsequently used to understand the scaling properties and the long-range correlations found in real DNA sequences [1, 11–13, 15]. In [7], Godrèche and Luck studied similar systems

---

✉ E. Ugalde  
ugalde@ifisica.uaslp.mx

C. Maldonado  
cesar.maldonado@ipicyt.edu.mx

L. Trejo-Valencia  
liliana@ifisica.uaslp.mx

<sup>1</sup> Instituto de Física, Universidad Autónoma de San Luis Potosí, Avenida Manuel Nava 6, Zona Universitaria, 78290 San Luis Potosí, Mexico

<sup>2</sup> División de Matemáticas Aplicadas, Instituto Potosino de Investigación Científica y Tecnológica, Camino a la Presa San José 2055, Lomas 4 sección, 78216 San Luis Potosí, Mexico

## Topical Review

# Quantum fluids of light in acoustic lattices

E A Cerda-Méndez<sup>1</sup> , D N Krizhanovskii<sup>2</sup>, M S Skolnick<sup>2</sup> and P V Santos<sup>3</sup>

<sup>1</sup> Universidad Autónoma de San Luis Potosí, Instituto de Investigación en Comunicación Óptica, Av. Karakorum 1470, Lomas 4a Secc. CP 78210, San Luis Potosí, Mexico

<sup>2</sup> Department of Physics and Astronomy, University of Sheffield, Sheffield S3 7RH, United Kingdom

<sup>3</sup> Paul-Drude-Institut für Festkörperelektronik, Leibniz-Institut im Forschungsverbund Berlin e.V., Hausvogteiplatz 5-7, 10117, Berlin, Germany

E-mail: [ecerda@cactus.iico.uaslp.mx](mailto:ecerda@cactus.iico.uaslp.mx)

Received 10 March 2017, revised 27 October 2017

Accepted for publication 1 December 2017

Published 28 December 2017

**Abstract**

In this topical review, we report on the recent advances on the manipulation of hybrid light–matter quasi-particles called exciton–polaritons and their quantum condensed phases by means of acoustic and static periodic potentials. Polaritons are a superposition of photons and excitons and form in optical microcavities with quantum wells embedded in it. They are low-mass bosons in the dilute limit and have strong inter-particle interactions inherited from the excitonic component. Their capability to form quantum-condensed phases at temperatures in the kelvin range and to behave like quantum fluids makes them very attractive for novel solid-state devices. Since their de Broglie wavelength is of the order of a few micrometers, polaritons can be manipulated using static or dynamic potentials with micrometer scales. We present here a summary of the techniques used to submit polaritons and their condensed phases to periodic potentials, with an emphasis in dynamic ones produced by surface acoustic waves. We discuss the interesting phenomena that occur under such a modulation, such as condensation in excited states of the Brillouin zone, fragmentation of a condensate, formation of self-localized wavepackets, and Dirac and massive polaritons in static hexagonal and kagome lattices, respectively. The different techniques explored open the way to implement polariton-based quantum simulators, nano-optomechanic resonators and polaritonic topological insulators.

Keywords: surface acoustic waves, exciton–polaritons, microcavities

(Some figures may appear in colour only in the online journal)

**1. Introduction**

The topic of strong light–matter interaction in solid state was re-launched in 1992 with the observation of exciton–polaritons in a semiconductor optical microcavity (MC) by Weisbuch *et al* (exciton–polaritons in bulk semiconductors were amply studied in 1960–1970) [1]. A MC is essentially a VCSEL structure: two reflectors embedding an active zone composed of a spacer containing ultra-thin material layers (quantum wells, QW) that confine excitons (figure 1(a)). In contrast to VCSELs, polariton MCs have a much higher

quality factor  $Q$  ( $10^3 \geq Q \geq 10^5$ ) [2]. Exciton–polaritons are thus quasi-particles with a very small effective mass ( $10^{-4}$ – $10^{-5}$  the free electron mass) generated by the superposition of photons and excitons. Since they are bosons in the dilute limit, it was quickly realized that polariton quantum condensed phases similar to Bose–Einstein condensates (BEC) could form in solid-state at much higher temperatures than in cold atom gases [3]. Evidence of quantum condensation of MC polaritons was promptly reported [4–6] and later, also the observation of what was called a polariton BEC by Kasprzak *et al* in 2006 [7] and Balili *et al* in 2007 [8].

## Wavelet characterization of hyper-chaotic time series

J.S. Murguía<sup>a</sup>, H.C. Rosu<sup>b</sup>, L.E. Reyes-López<sup>c</sup>, M. Mejía-Carlos<sup>c</sup>, and C. Vargas-Olmos<sup>c</sup>

<sup>a</sup> Facultad de Ciencias, Universidad Autónoma de San Luis Potosí (UASLP),  
Alvaro Obregón 64, 78000 San Luis Potosí, S.L.P., México.

<sup>b</sup> IPICYT, Instituto Potosino de Investigación Científica y Tecnológica,  
Camino a la presa San José 2055, Col. Lomas 4a Sección, 78216 San Luis Potosí, S.L.P., México.

<sup>c</sup> Instituto de Investigación en Comunicación Óptica, UASLP,  
Alvaro Obregón 64, 78000 San Luis Potosí, S.L.P., México.

Received 5 November 2017; accepted 19 January 2018

A wavelet scaling numerical characterization of time series based on the variance of the wavelet coefficients is used for three well-known four-dimensional and one five-dimensional hyper-chaotic systems. We report several scaling behaviors for the variables of these hyper-chaotic systems.

*Keywords:* Hyper-chaotic time series; discrete wavelet transform; wavelet variance; scaling analysis.

En este trabajo se realiza una caracterización de escala numérica de series de tiempo hiper-caóticas basada en la varianza de los coeficientes ondeleta de tres sistemas hiper-caóticos conocidos de cuatro-dimensiones y uno de cinco-dimensiones. Se reportan los diferentes comportamientos de escala de las variables de estos sistemas hiper-caóticos.

*Descriptor:* Series de tiempo hiper-caóticas; transformada ondeleta discreta; varianza ondeleta; análisis de escala.

PACS: 05.45.-a; 05.45.Tp

### 1. Introduction

The wavelet transform (WT) is a mathematical tool for analyzing (decomposing) or synthesizing (reconstructing) a wide variety of generic signals at different frequencies and with different resolutions. In the wavelet analysis, a signal is decomposed into a type of functions called wavelets, which are translated and scaled versions of a finite-length and fast-decaying oscillating waveform. The latter is usually referred to as the analyzing wavelet basis function, or simply the mother wavelet. Similar to its preceding Fourier analysis, the wavelet analysis also contains various, closely-related forms of its transform, namely the continuous wavelet transform, the wavelet series, and the orthonormal discrete wavelet transform or, for short, the discrete wavelet transform (DWT). However, the most common choice to perform the analysis and synthesis of the original signal is the DWT because of the enormous versatility for computational calculations offered through its multiresolution filter bank structure [1, 2]. Just as in the other existent formats of the wavelet transform, the DWT is endowed with temporal resolution as a unique key advantage over its Fourier transform counterpart which allows to capture both the frequency and location information of the raw signal being processed in this way.

To the best of our knowledge, the class of hyper-chaotic systems, *i.e.*, those dynamical systems having at least two positive Lyapunov exponents, have not been directly studied by means of wavelet transforms. This motivated us to provide here a wavelet scaling analysis of four hyper-chaotic systems, of which three are four-dimensional – Chen, Chua, and Rössler – and one is a recently introduced five-dimensional system. All these systems are reviewed in Sec. 2, where we briefly present their systems of equations and attractors for

values of the parameters corresponding to the hyper-chaotic regime. Section 3 is devoted to a short description of the DWT. The main results are in Sec. 4, where we apply the wavelet analysis to the time series (TS) of the variables of these systems when they are in the hyper-chaotic regime. The paper ends up with a short conclusion section.

### 2. Hyper-chaotic systems

This section is devoted to a brief presentation of the four hyper-chaotic systems which we will consider in this work. These systems, despite their relative simplicity, exhibit a more complex dynamics than the chaotic systems, and they have received wide coverage in different areas of mathematics, physics, and engineering, among others [3–9].

#### 2.1. Hyper-chaotic Chen system

The hyperchaotic dynamics of Chen's system is modeled by the set of differential equations [4, 6]

$$\begin{aligned}\dot{x} &= a(y - x), \\ \dot{y} &= x(d - z) + cy - w, \\ \dot{z} &= xy - bz, \\ \dot{w} &= x + k,\end{aligned}\tag{1}$$

where  $a, b, c, d$  and  $k$  are parameters of the system. If  $a = 36$ ,  $b = 3$ ,  $c = 28$ ,  $d = -16$  and  $-0.7 \leq k \leq 0.7$ , the system (1) is in the hyper-chaotic regime. In fact, to check the existence of hyper-chaos, there must be at least two positive Lyapunov exponents. The numerically calculated exponents

# Application of dynamical system theory in LC harmonic oscillator circuits: A complement tool to the Barkhausen criterion

International Journal of Electrical Engineering  
Education  
0(0) 1–15

© The Author(s) 2018


Reprints and permissions:

[sagepub.co.uk/journalsPermissions.nav](http://sagepub.co.uk/journalsPermissions.nav)

DOI: 10.1177/0020720918770140

[journals.sagepub.com/home/ije](http://journals.sagepub.com/home/ije)



Pablo Salas-Castro<sup>1</sup> ,  
Fines Delgado-Aranda<sup>1</sup>,  
Edgar Tristán-Hernández<sup>1</sup>,  
Roberto C Martínez-Montejano<sup>2</sup>,  
J S Murguía<sup>3</sup> and  
Isaac Campos-Cantón<sup>1</sup>

## Abstract

There are different types of electronic oscillators that have a wide variety of applications in areas such as computing, audio, communication, among others. One of these is the harmonic oscillators that generate an output sinusoidal signal. Due to the advantages of these, this paper proposes a methodology based on an analysis based on the dynamical system theory. This provides undergraduates a useful tool for a better understanding of the harmonic oscillators in order to design and implement accurately this kind of circuits. This tool complements the widely recognized Barkhausen criterion, which is a mathematical condition that must be satisfied by linear feedback oscillators. The analysis based on the dynamical system theory consists of obtaining a state matrix and its eigenvalues from the mathematical model of the oscillator circuits. The eigenvalues are adjusted to get an oscillator system, thus from this way, a set of

<sup>1</sup>Instituto de Investigación en Comunicación Óptica, Facultad de Ciencias, UASLP, México

<sup>2</sup>Unidad Académica Multidisciplinaria Zona Media, UASLP, México

<sup>3</sup>Facultad de Ciencias, UASLP, México

## Corresponding author:

Pablo Salas-Castro, Instituto de Investigación en Comunicación Óptica, Facultad de Ciencias, UASLP, San Luis Potosí, SLP, México.

Email: [iepablosalas@hotmail.com](mailto:iepablosalas@hotmail.com)